1980

A finite-element simulation of pulsatile flow in flexible tubes

Elkana Rooz
Iowa State University

INFORMATION TO USERS

This was produced from a copy of a document sent to us for microfilming. While the most advanced technological means to photograph and reproduce this document have been used, the quality is heavily dependent upon the quality of the material submitted.

The following explanation of techniques is provided to help you understand markings or notations which may appear on this reproduction.

1. The sign or "target" for pages apparently lacking from the document photographed is "Missing Page(s)". If it was possible to obtain the missing page(s) or section, they are spliced into the film along with adjacent pages. This may have necessitated cutting through an image and duplicating adjacent pages to assure you of complete continuity.

2. When an image on the film is obliterated with a round black mark it is an indication that the film inspector noticed either blurred copy because of movement during exposure, or duplicate copy. Unless we meant to delete copyrighted materials that should not have been filmed, you will find a good image of the page in the adjacent frame.

3. When a map, drawing or chart, etc., is part of the material being photographed the photographer has followed a definite method in "sectioning" the material. It is customary to begin filming at the upper left hand corner of a large sheet and to continue from left to right in equal sections with small overlaps. If necessary, sectioning is continued again—beginning below the first row and continuing on until complete.

4. For any illustrations that cannot be reproduced satisfactorily by xerography, photographic prints can be purchased at additional cost and tipped into your xerographic copy. Requests can be made to our Dissertations Customer Services Department.

5. Some pages in any document may have indistinct print. In all cases we have filmed the best available copy.

University
Microfilms
International

300 N. ZEEB ROAD, ANN ARBOR, MI 48106
18 BEDFORD ROW, LONDON WC1R 4EJ, ENGLAND

ROOZ, ELKANA

A FINITE-ELEMENT SIMULATION OF PULSATILE FLOW IN FLEXIBLE TUBES

Iowa State University PH.D. 1980

PLEASE NOTE:

In all cases this material has been filmed in the best possible way from the available copy. Problems encountered with this document have been identified here with a check mark ✓.

1. Glossy photographs ✓
2. Colored illustrations _____
3. Photographs with dark background ✓
4. Illustrations are poor copy _____
5. Print shows through as there is text on both sides of page _____
6. Indistinct, broken or small print on several pages _____
7. Tightly bound copy with print lost in spine _____
8. Computer printout pages with indistinct print _____
9. Page(s) _____ lacking when material received, and not available from school or author
10. Page(s) _____ seem to be missing in numbering only as text follows
11. Poor carbon copy _____
12. Not original copy, several pages with blurred type _____
13. Appendix pages are poor copy _____
14. Original copy with light type _____
15. Curling and wrinkled pages _____
16. Other _____

A finite-element simulation of pulsatile flow in flexible tubes

by

Elkana Rooz

A Dissertation Submitted to the

Graduate Faculty in Partial Fulfillment of the

Requirements for the Degree of

DOCTOR OF PHILOSOPHY

Departments: Engineering Science and Mechanics
Biomedical Engineering
Co-majors: Engineering Mechanics
Biomedical Engineering

Approved:

Signature was redacted for privacy.

Signature was redacted for privacy.

In Charge of Major Work

Signature was redacted for privacy.

Professor-in-charge,
Program in Biomedical Engineering

Signature was redacted for privacy.

For the Major Department

Signature was redacted for privacy.

For the Graduate College

Iowa State University
Ames, Iowa

1980

TABLE OF CONTENTS

GENERAL INTRODUCTION

One common form of arterial disease results in a localized constriction of a major artery (stenosis). With the development of a stenosis, the blood perfusion to the vascular bed distal of the artery is altered, and consequently, irreversible damages to vital organs supplied by this artery can occur. One of the reasons that a developing stenosis is difficult to detect, and stenosis effects on the blood flow are difficult to assess, is that the problem of blood motion in a partially occluded artery is not completely understood. Thus, the purpose of this investigation is to study the motion of pulsatile flow in flexible tubes and to evaluate the relationship between the pulsatile pressure, pulsatile flow and the physical properties of the elastic tube. The approach used involves the development of two mathematical models for pulsatile flow; one for an unobstructed flexible tube, and the other for an obstructed flexible tube. Solutions for pressures and flows are obtained from the model equations by employing a numerical method since the model partial differential equations are nonlinear in nature and have no available analytical solution. The numerical method used is the finite-element method which is applicable to nonlinear problems and can handle various boundary conditions and complex geometries with relative ease.

Explanation of Dissertation Format

The dissertation is divided into two major sections which are written in the form of papers to be submitted to a journal and three appendices. In the first paper, emphasis is placed on the study of pulsatile flow in

an unobstructed tube. The second paper involves the study of pulsatile flow in an obstructed tube. Appendix A includes further details on the finite-element development for the unobstructed tube and Appendix B includes details on the method of solution of the obstructed tube equations. Appendix C contains photographs of the laboratory system used to obtain the experimental data.

No additional literature is cited in this introduction since references relevant to this problem are included in sections one or two. The portion of the major work described herein was contributed by the author of this dissertation. However, this study could not have been satisfactorily completed without the indispensable guidance and supervision of Professors D. F. Young and T. R. Rogge.

A FINITE-ELEMENT SIMULATION OF PULSATILE FLOW IN FLEXIBLE TUBES--PART-I. FLOW IN AN UNOBSTRUCTED TUBE

Elkana Rooz
Donald F. Young
Thomas R. Rogge

From the Department of Engineering Science and Mechanics and the Biomedical Engineering Program, Iowa State University, Ames, IA 50011

Supported by the Engineering Research Institute of Iowa State University.

ABSTRACT

A finite-element model for pulsatile flow in a flexible straight tube is developed. The model is based on the continuity equation, the one-dimensional momentum equation, and an equation of state relating tube cross-sectional area to pressure. Two versions of the model are solved numerically. One model is based on complete linearization of equations, whereas, the second model is based on a nonlinear equation of state. In both cases, the applicability of the model is checked by comparing predicted waveforms of pressure and flow with corresponding experimental results. The experimental data are obtained from *in vitro* measurements on a mechanical system which is arranged to record instantaneous pressures and flows. It is found that the linear model satisfactorily predicts the waveforms of pressure and flow under a variety of boundary conditions. However, further significant improvement of the predicted waveforms is achieved through the solution of a model which includes a nonlinear equation of state.

NOMENCLATURE

A	Cross-sectional area of vessel
A_0	Average cross-sectional area at average pressure p_0
$[A]$	Coefficient matrix of linear terms in a model
a	Half length of an element
$[B]$	Coefficient matrix of nonlinear terms in a model
b	Half of a time step
C_0	Constant compliance
C_0', C_1, C_1'	Coefficients of nonconstant compliance
D	Vessel diameter
f	Frequency of waveform
$[N]$	Shape function matrix
p	Pressure
p_i	Nodal pressure
Q	Flow
Q_i	nodal flow
$\{\delta\}_e$	Vector of element degrees of freedom
r	Dimensionless axial length coordinate
s	Dimensionless time coordinate
t	Time
x	Axial length coordinate
Z	Peripheral resistance
$\{\delta\}$	Vector of global degrees of freedom
μ	Fluid viscosity
ρ	Fluid density

τ_0 Wall shearing stress

INTRODUCTION

The problem of pulsatile flow in a flexible tube has been considered by numerous investigators primarily because of its applicability to the study of arterial blood flow. Cox [1] in a review paper notes twenty-one previous studies which use a linear propagation model to obtain a solution for this problem. The common features of all of these early studies were the assumptions that the tube was straight, the vessel wall was linearly elastic, and the contribution of the convective acceleration in the momentum equation was negligible. The most significant difference between them was the different assumptions made with respect to the behavior of the vessel wall. If the axial motion of the wall is constrained, the linear model further reduces to a set of equations [2] which is analogous to those used in transmission line theory. The disadvantage of the linear models is that they fail to account for the effects of a nonlinear wall behavior and of a tapering tube. The attempt to incorporate these effects into an overall solution led to the development of nonlinear models [3,4]. All the proposed nonlinear models are based on equations for one-dimensional flow including the continuity equation and the momentum equation, and a third equation which relates the cross-section area of the tube with the pressure (equation of state). Generally, the form of the equation of state is based on experimental data, and the nature of the equation of state obviously depends on the vessel wall material. For arteries, an appropriate equation of state is not well-established, and frequently some sort of exponential relationship between the cross-sectional area and pressure is used [3,6].

To complete the formulation of any model, two boundary conditions are specified, one at the proximal end of the tube, and the other at the distal end. Commonly these conditions are prescribed as a proximal pressure and a distal impedance, or by the assumption that the tube is infinite. Analytical solutions for the linear model are available [1,2,3], whereas for the nonlinear model, the system of equations must be solved numerically. The methods that have been frequently used are the method of characteristics [7] and the method of finite difference [6].

The concerns of this study are the development of a finite-element model for the study of pulsatile flow in a flexible tube, and to investigate the applicability of the model experimentally. The finite-element method has been applied to a variety of engineering problems, and it is believed that it offers a viable alternative to other methods for the study of blood flow. Both linear and nonlinear models are examined with respect to: (a) agreement between the predicted and the corresponding experimental waveforms under a variety of boundary conditions; and (b) the sensitivity of the solutions to different parameters, such as the radius of the tube and tube compliance.

GOVERNING EQUATIONS

The motion of the pulsating flow is largely dominated by the distensibility of the tube wall, and by the forces due to the local acceleration and axial pressure gradient. The motion is influenced to a lesser degree by forces due to friction and convective acceleration. The effects of friction and convective acceleration, which are functions of the velocity profile, can be approximated by terms which depend on the flow rate, and it is expected that the nature of these approximations will have little effect on the overall solution. The laws of conservation of mass and momentum yield,

$$\frac{\partial Q}{\partial x} + \frac{\partial A}{\partial t} = 0 \tag{1}$$

and

$$\frac{\partial Q}{\partial t} + \frac{\partial}{\partial x}\int_A V^2 dA = -\frac{A}{\rho}\frac{\partial p}{\partial x} + \frac{\tau_o \pi D}{\rho} \tag{2}$$

The system is completed by an equation of state,

$$A = A(p,x) \tag{3}$$

Several models for the wall shear stress are offered in the literature [5]. As mentioned above, since it does not appear to be highly significant which model is used, the simplest model is adopted for the present study. It is given by the expression for a wall shear stress under conditions of steady and uniform flow, i.e.,

$$\tau_o = -\frac{8\mu Q}{DA} \tag{4}$$

Although the convective acceleration can be approximated by the expression,

$$\frac{\partial}{\partial x}\int_A V^2 dA = \frac{\partial}{\partial x}\left(\frac{\lambda Q^2}{A}\right) \tag{5}$$

where λ is a parameter which depends on the velocity profile (λ is one for uniform profile and four thirds for parabolic profile), this term will generally be small and has been neglected in the present study. However, alternate forms for the wall shear stress and the inclusion of the convective acceleration into the finite-element model if deemed

[redacted]

in two

respe cause of

the the

pres uming the

follo of state

is lin

A(p (6)

where $C_0(x)$ cation, and

$A_0(x)$ is the cr For a straight tube

with no tapering $A_0(x)$ (b) The change in the

cross-sectional area is small compared with the cross-section itself, i.e.,

$$\left|\frac{A(p,x) - A_0(x)}{A_0(x)}\right| \ll 1 \tag{7}$$

and consequently, the cross-sectional area which appears in the coefficients of the momentum equation is approximated by the average cross-

$$\frac{\partial}{\partial x}\int_A V^2 dA = \frac{\partial}{\partial x}\left(\frac{\lambda Q^2}{A}\right) \tag{5}$$

where λ is a parameter which depends on the velocity profile (λ is one for uniform profile and four thirds for parabolic profile), this term will generally be small and has been neglected in the present study. However, alternate forms for the wall shear stress and the inclusion of the convective acceleration term could be incorporated into the finite-element model if deemed necessary.

Linearized Model

The system of equations (1), (2) and (3) may be nonlinear in two respects: first, because of the convective term, and second, because of the possible nonlinear dependence of the cross-sectional area on the pressure. The system was linearized by Westerhof et al. [8] by assuming the following: (a) Over the operating pressure range, the equation of state is linear and of the form,

$$A(p,x) - A_0(x) = C_0(x)(p - p_0) \tag{6}$$

where $C_0(x)$ is a constant compliance $(\partial A/\partial p)$ at a given location, and $A_0(x)$ is the cross-sectional area at the pressure p_0. For a straight tube with no tapering $A_0(x)$ and $C_0(x)$ are constant. (b) The change in the cross-sectional area is small compared with the cross-section itself, i.e.,

$$\left|\frac{A(p,x) - A_0(x)}{A_0(x)}\right| \ll 1 \tag{7}$$

and consequently, the cross-sectional area which appears in the coefficients of the momentum equation is approximated by the average cross-

section $A_0(x)$. (c) The convective term in the momentum equation is small and can be omitted. The equations of the linear model are therefore

$$\frac{\partial Q}{\partial x} + C_0 \frac{\partial p}{\partial t} = 0 \tag{8}$$

and

$$\frac{\rho}{A_0} \frac{\partial Q}{\partial t} + \frac{\partial p}{\partial x} + \frac{8\pi\mu}{A_0^2} Q = 0 \tag{9}$$

Nonlinear Model

The assumptions that the change in the cross-sectional area is small compared with the cross-section itself, and that the convective term is small are considered to be valid also for the nonlinear model in the present study. However, the equation of state is assumed to have a quadratic polynomial form. For a straight tube, the equation of state is

$$A - A_0 = C_0(p - p_0) + C_1(p - p_0)^2 \tag{10}$$

where C_0 and C_1 are constants. This assumed form is based on experimental data to be described in a following section. The equations of the nonlinear model are therefore

$$\frac{\partial Q}{\partial x} + C_0' \frac{\partial p}{\partial t} + C_1' p \frac{\partial p}{\partial t} = 0 \tag{11}$$

and

$$\frac{\rho}{A_0} \frac{\partial Q}{\partial t} + \frac{\partial p}{\partial x} + \frac{8\pi\mu}{A_0^2} Q = 0 \tag{12}$$

where

$$C_0' = C_0 - 2C_1 p_0 \tag{13a}$$

and

$$C_1' = 2C_1 \tag{13b}$$

Equations (12) and (13) constitute the basic flow equations for which the finite-element method is applied. It is evident that the linear model is easily obtained from equation (12) by setting the coefficient C_1' equal to zero. To complete the mathematical formulation of the problem, it is necessary to specify proximal and distal boundary conditions. The proximal boundary condition can be either the flow or pressure, specified as function of time. Similarly, the distal boundary condition can be a specified flow or pressure or alternatively, a terminal resistance can be used for this boundary condition.

NUMERICAL METHOD

The numerical method used in this study is the finite-element method [9,10] which is equally applicable to linear or nonlinear equations, and which can handle various types of boundary conditions with relative ease.

The method was applied on both the time and the space dimensions to reduce the system of partial differential equations (12) and (13) to a system of algebraic equations. Each element has a rectangular shape (Figure 1), and its horizontal and vertical sides correspond to a length and a time step, respectively. A local coordinate system x and t and the corresponding dimensionless coordinate system r and s are attached to the centroid of the element. The relationships among x, t, r, and s are

$$r = \frac{x}{a}$$

and

$$s = \frac{t}{b}$$

where a and b are half of the length and time steps, respectively. Within the element, the pressures and flows are prescribed by

$$\begin{Bmatrix} P \\ Q \end{Bmatrix} = [N]\{\delta\}_e \tag{14}$$

where [N] is the shape function matrix given by,

$$[N] = \begin{bmatrix} N^1 \\ N^2 \end{bmatrix} = \begin{bmatrix} N_1,0,N_2,0,N_3,0,N_4,0 \\ 0,N_1,0,N_2,0,N_3,0,N_4 \end{bmatrix}$$

$$N_i = \frac{1}{4}(1 + rr_i)(i + ss_i),\ r_i = \pm 1,\ s_i = \pm 1,\ i = 1, 2, 3, 4$$

and

$$\{\delta\}_e = [p_1, q_1, p_2, \ldots, p_4, q_4]^T$$

Figure 1. Element discretization representing total tube length and one time increment

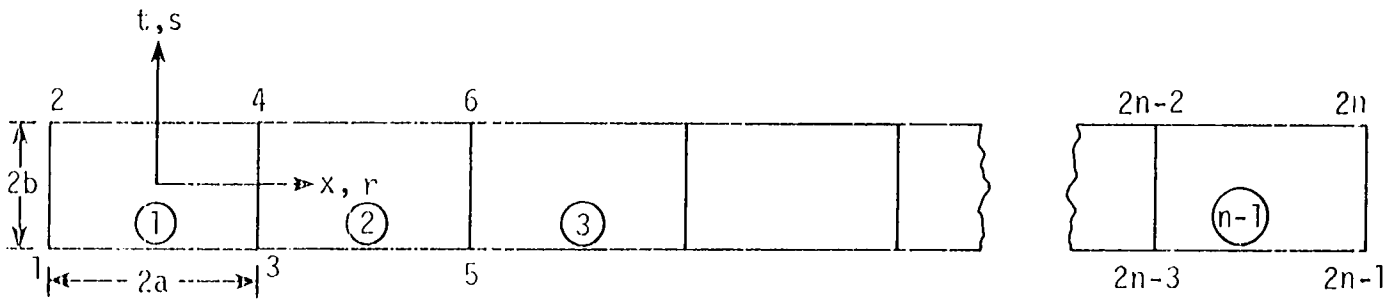
t, s
x, r
2
4
6
2b
1
2a
3
5
2n-2
2n
n-1
2n-3
2n-1

Substitution of the pressure and flow representation into equations (12) and (13) yields

$$L_1 = [N^2]_r r_x \{\delta\}_e + C_0'[N^1]_s s_t \{\delta\}_e + C_1'[N^1]\{\delta\}_e [N^1]_s s_t \{\delta\}_e \tag{15}$$

$$L_2 = \frac{\rho}{A_0}[N^2]_s s_t \{\delta\}_e + [N^1]_r r_x \{\delta\}_e + \frac{8\pi\mu}{A_0^2}[N^1]\{\delta\}_e \tag{16}$$

where

$$[N^2]_r = \frac{\partial [N^2]}{\partial r},\ r_x = \frac{\partial r}{\partial x},\ [N^1]_s = \frac{\partial [N^1]}{\partial s},\ \text{etc.}$$

The element equations are obtained by the use of the Galerkin method,

$$\int_A ab[N]^T L_1 dA + \int_A ab[N]^T L_2 dA = 0,\ dA = dr\ ds$$

The assemblage process is employed for a line of elements (Figure 1) to obtain the global set of equations which can be written as

$$[A]\{\delta\} + [B]\{\delta\} = 0 \tag{17}$$

where

$$\{\delta\} = [p_1, q_1, p_2, \cdots, p_{2n}, q_{2n}]^T$$

and [A] is a matrix of constant coefficients, and corresponds to the linear terms in the model. Matrix [B] includes variable coefficients which are function of the vector $\{\delta\}$ and it corresponds to the nonlinear terms in the model.

Initial Conditions

In each time step the nodal values of the pressures and the flows at the bottom of the line element in Figure 1, i.e., the pressures and flows that carry an odd index, are specified from the solution of the previous step. Their values are substituted into the vector $\{\delta\}$. Then they are

multiplied by the corresponding coefficients in the matrices [A] and [B], and the summation of the products are carried to the right side of the equation to form a force vector {f}. Consequently, the number of unknowns in the matrix equation reduces to one-half of the original number of unknowns, which means that only half of the number of the original equations is needed to obtain a solution. A new matrix equation is formed by selecting the equations of the original system that correspond to the nodes with the unknown pressures and flows. The new matrix equation is written in the following form:

$$[A^*]\{\delta^*\} + [B^*]\{\dot{\delta}^*\} = \{f^*\} \tag{18}$$

where the superscript * denotes the reduced form. It is noted that [A*] and [B*] are banded nonsymmetrical matrices with a bandwidth of 4. For the first time step, the initial conditions are specified by setting the force vector {f*} to zero, which means that the solution starts and progresses through a transient period until it converges into a steady-state mode.

Boundary Conditions

The boundary condition at the proximal end is specified by the instantaneous value of either the pressure or the flow at node 2. Similarly, the boundary condition at the distal end can be specified by either the instantaneous value of the pressure or the flow at node 2n, or alternatively by a terminal resistance. For a boundary condition which is specified by either pressure or flow the treatment is to substitute its value into {δ*}, multiply it by the proper coefficients in the matrices

[A*] and [B*], and carry the summation of the products to the right side of the equation. Also, the equation corresponding to this boundary condition is replaced by an equation of the form $\delta_i^* = \delta_i^*$ where δ_i^* is the boundary condition. With respect to a boundary condition specified by the terminal resistance, the treatment is to substitute for the 2n-th equation in the matrix equation, by an algebraic equation which relates the pressure and flow at node n with the terminal resistance.

Solution of the Algebraic Equations

As noted previously, the linearized model is obtained by setting the constant C_1' equal to zero, which in turn yields a value of zero for the matrix [B*]. The solution for the linear model is obtained by employing a linear system solver routine for a banded nonsymmetrical matrix which is based on the Gauss Elimination Method. With respect to the nonlinear system, an iterative procedure is used. In each iteration, the following linear system is solved

$$[A^*]_m\{\delta^*\}_m = \{f^*\} - [B^*]_{m-1}\{\delta^*\}_{m-1} \tag{19}$$

where m is the iteration number. The first guess for $\{\delta^*\}$ in time step k is specified by the solution of $\{\delta^*\}$ in time step k-1. The iteration procedure is continued until the iterations are assumed to converge. The criterion for convergence is given by

$$\left|\frac{(\delta_i^*)_{m-1}}{(\delta_i^*)_m}\right| < \varepsilon \qquad i = 1, 2, \ldots, 2n$$

where 2n is the number of nodes, and ε is a small real number. This iterative procedure proved to work well for the solution of the nonlinear

model. It is simple to use, and it is relatively low on computer time consumption.

EXPERIMENTAL MODEL AND INPUT DATA

A schematic of the basic flow system is shown in Figure 2. The main three components of the mechanical system are: (a) a pulsatile pump with a variable piston stroke driven by a variable speed motor; (b) a flexible, thin-walled latex tube; and (c) a peripheral resistance consisting of a number of small diameter polyethylene tubes connected in parallel. In this system, the flow is controlled by the piston stroke, the pressure by the peripheral resistance, and the frequency by the motor speed. The pressures at the inlet and the outlet of the tube are measured by two pressure transducers (Statham P23Db) which are connected directly to the system through rigid hypodermic needles. With the direct connection, the natural frequency of the transducers is high (180 Hz is specified by the manufacturer for 50 mm long 20 gage needle), and is well above the tenth harmonic frequency of any measured wave. The flows are measured with electromagnetic flowmeters (Biotronix BL-610) with two 3-mm cannulating probes which are connected to the inlet and the outlet of the tube. The dynamic response of the flowmeter was checked electronically and found to be flat to approximately 30 Hz with linear phase shift of 3.6%/Hz.

The calibration of the pressure transducers and the flow probes is obtained by means of static pressure and steady flow measurements, respectively. The pressures and flows are recorded on a six channel Grass Polygraph and also sampled, digitized and calibrated by a PDP 8/e digital computer with a built-in A/D converter and a built-in clock. The use of the computer provides the advantages of measurement with high accuracy, high sampling rate, and better control of the experimental course through

Figure 2. Schematic of the experimental flow system and instrumentation

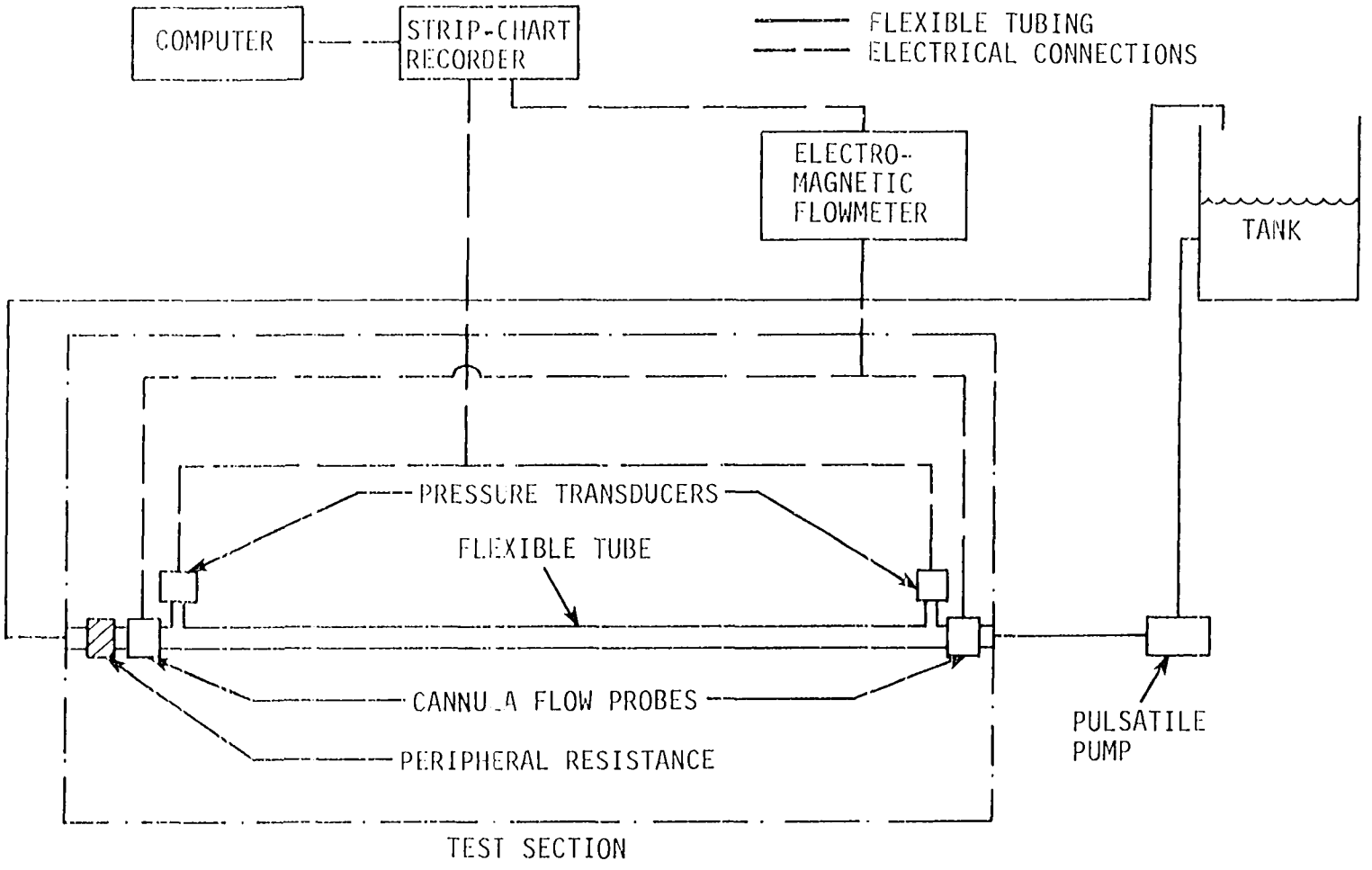
COMPUTER
STRIP-CHART RECORDER
FLEXIBLE TUBING
ELECTRICAL CONNECTIONS
ELECTRO-MAGNETIC FLOWMETER
TANK
PRESSURE TRANSDUCERS
FLEXIBLE TUBE
CANNULA FLOW PROBES
PERIPHERAL RESISTANCE
PULSATILE PUMP
TEST SECTION

a fast calibration and a fast display of the recorded data. For each measured waveform, Fourier harmonic moduli were obtained, and subsequently, the Fourier series representing the experimental waveforms used for the numerical solutions.

Input Parameters

Through all the experiments, physiological saline with a density of 997 kg/m^3 and viscosity of 8.9×10^{-4} Pa·s was used. Simultaneous recordings of the proximal and distal pressures and flows were obtained for four different frequencies (see Table 1). Data were sampled over a period of five seconds with a rate of one hundred samples per second, and subsequently, transferred to a high speed digital computer (Itel AS6). Frequency parameters $D\sqrt{\omega\rho/\mu}/2$, where ω is the angular frequency based on the fundamental frequency of the pulsation, and Reynolds numbers $\rho VD/\mu$ based on the peak and average velocities for all tests are given in Table 1.

The data for the calculation of the tube compliance were obtained by blocking the tube at both ends and injecting saline into it in increments of volume of 100 mm^3. In each step, the increase in pressure was recorded, and the corresponding increase in cross-sectional area calculated by dividing the step volume by the fixed length of the tube. The results of these tests are shown in Figure 3 where the slope of the curve represents the compliance. The constant compliance was obtained by fitting the best straight line to the data in the operating pressure range. The coefficients for the nonlinear case were calculated by fitting a quadratic curve to the data over the operating pressure range (see Figure 3). Values for

Table 1. Summary of experimental system parameters

Frequency Hz f	Frequency parameter, $D\sqrt{\omega\rho/\mu}/2$	Reynolds number $\rho VD/\mu$		Area, A_0 m^2	Compliance			Peripheral resistance, Z $N \cdot s/m^5$
					Constant, C_0 m^4/N	Nonconstant		
		Mean	Peak			C_0' m^4/N	C_1' m^6/N^2	
0.40	5.62	418	1085	$3.53\ 10^{-5}$	3.2×10^{-10}	1.7×10^{-10}	0.5×10^{-14}	7.0×10^{9}
0.62	6.97	375	1253	$3.50\ 10^{-5}$	3.1×10^{-10}	1.0×10^{-10}	0.7×10^{-14}	6.9×10^{9}
0.98	8.81	387	1772	$3.53\ 10^{-5}$	3.2×10^{-10}	1.0×10^{-10}	0.7×10^{-14}	6.8×10^{9}
1.49	10.89	410	1782	$3.55\ 10^{-5}$	3.3×10^{-10}	1.0×10^{-10}	0.7×10^{-14}	6.8×10^{9}

Figure 3. Experimentally determined relationship between the tube cross-sectional area and transmural pressure

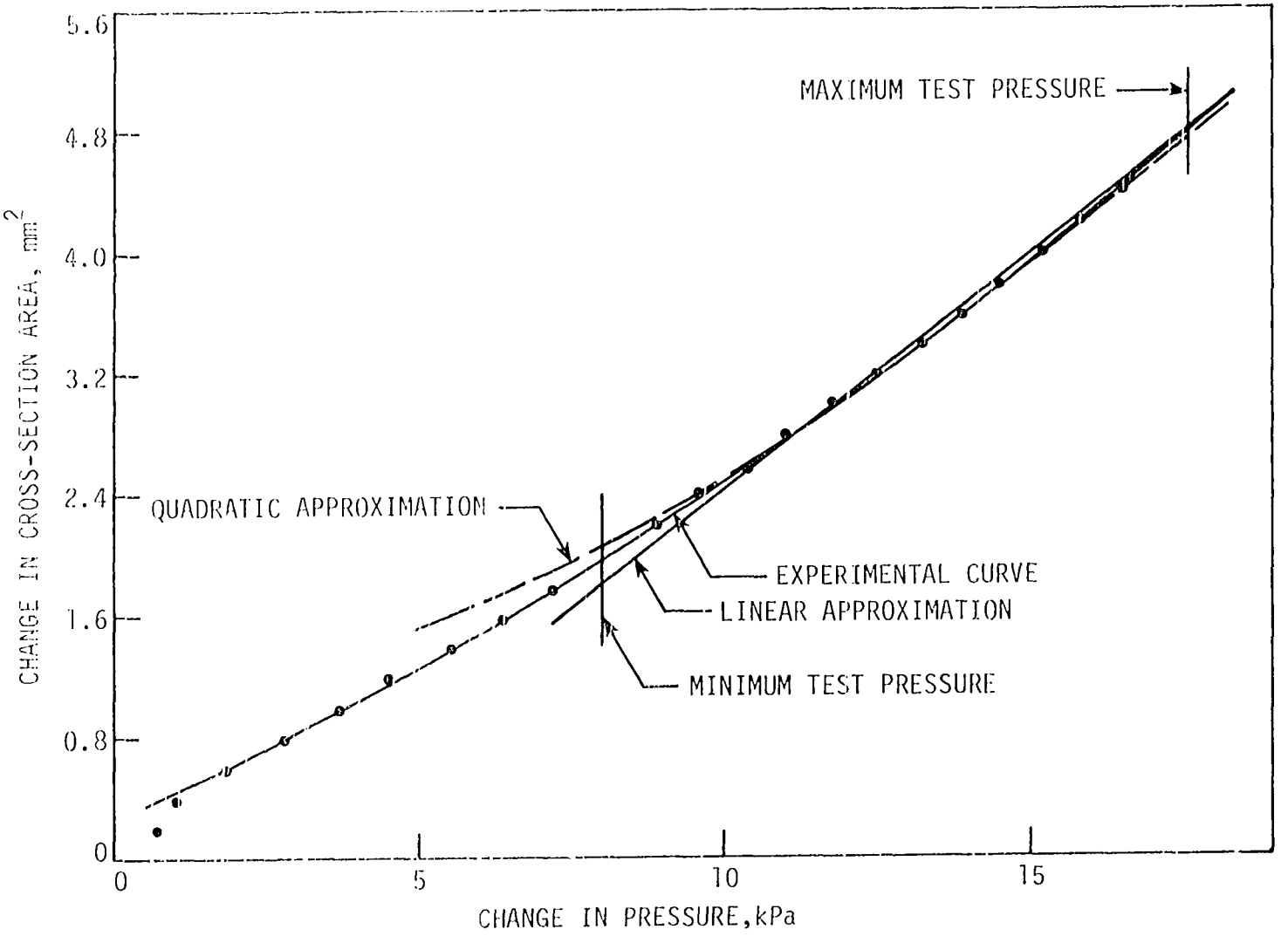
5.6
4.8
4.0
3.2
2.4
1.6
0.8
0
CHANGE IN CROSS-SECTION AREA, mm2
0
5
10
15
CHANGE IN PRESSURE, kPa
MAXIMUM TEST PRESSURE
QUADRATIC APPROXIMATION
EXPERIMENTAL CURVE
LINEAR APPROXIMATION
MINIMUM TEST PRESSURE

the compliances and the nominal cross-sectional areas, A_0, are given in Table 1. These values varied slightly for the different tests, since the operating pressure range was slightly different for each test.

The instantaneous peripheral resistance was obtained from the ratio of the instantaneous distal pressure to flow. Calculation of the instantaneous resistance indicated an insignificant variation with respect to either frequency or time, indicating that the peripheral resistance could be approximated by a "pure" resistance. Thus, the instantaneous values were averaged over a cycle to give a mean resistance, Z, which was used as one of the input boundary conditions. Values of Z are also given in Table 1.

RESULTS AND DISCUSSION

To check the validity of the basic flow model and the finite-element analysis, computer solutions for a variety of sets of boundary conditions and frequencies of oscillation were obtained from both the linearized and the nonlinear versions of the model. The predicted waveform of either pressure or flow was compared with the corresponding experimentally measured waveform. Proximal and distal boundary conditions utilized include: pressure-flow (p-Q), pressure-pressure (p-P), flow-flow (Q-Q), pressure-resistance (p-Z), and flow-resistance (Q-Z). Measured values for these boundary conditions were used as input to the computer model along with specified values of fluid density and viscosity, vessel compliance, mean cross-sectional area of vessel, and length of vessel. In general, the waveforms predicted from the linear model were in good agreement with the experimental results as illustrated in Figure 4. Some discrepancy is noted immediately preceding peak flow. This small difference between the measured and the predicted flows is due primarily to the assumption of constant vessel compliance. Use of the nonlinear model to obtain a solution for the same boundary conditions and frequency of oscillation reduces the discrepancy between the calculated and the experimental waveforms, as shown in Figure 5. It was also found that the use of the nonconstant compliance dampens resonance effects which may appear in the waveform predicted from the linear model. Thus, for example, the experimental data for the linear model were reconstructed from the first five harmonics (Figure 4) since higher harmonics were found to produce resonance, whereas

Figure 4. Comparison of proximal flow predicted from the linear model with measured flow. Pressure-peripheral resistance boundary conditions with parameters: $A_0 = 3.50\times10^{-5}m^2$, $C_0 = 3.1\times10^{-10}m^4/N$, $\rho = 997\ kg/m^3$, $\mu = 8.9\times10^{-4}\ Pa\cdot s$, and $f = 0.62\ Hz$

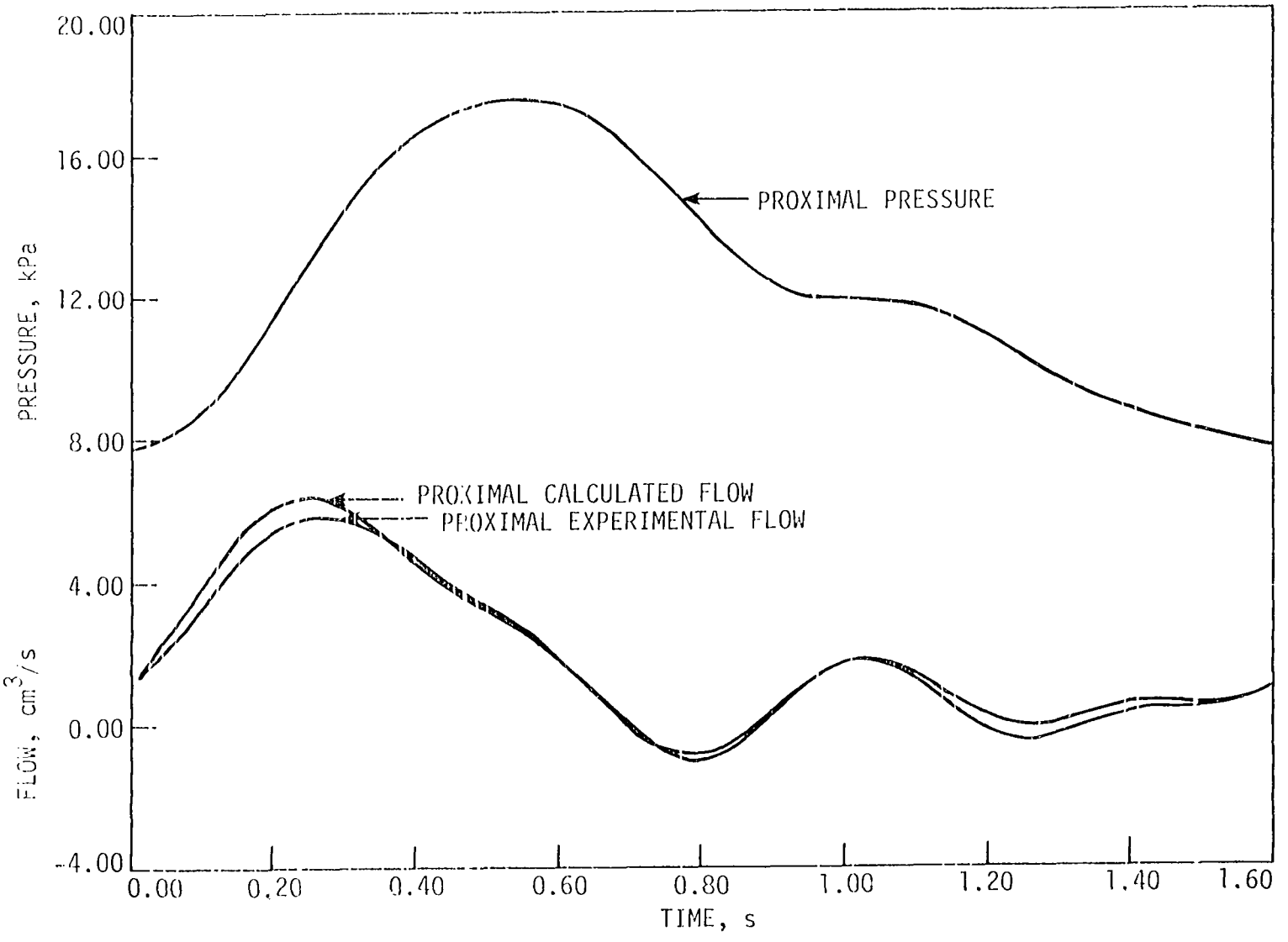
20.00
16.00
12.00
8.00
4.00
0.00
-4.00
PRESSURE, kPa
FLOW, cm3/s
PROXIMAL PRESSURE
PROXIMAL CALCULATED FLOW
PROXIMAL EXPERIMENTAL FLOW
0.00
0.20
0.40
0.60
0.80
1.00
1.20
1.40
1.60
TIME, s

Figure 5. Comparison of proximal flow predicted from the nonlinear model with measured flow. Pressure--peripheral resistance boundary conditions with parameters: $A_0 = 3.50\times10^{-5}m^2$, $C_0^1 = 1.0\times10^{-10}m^4/N$, $C_1^1 = 0.7\times10^{-14}m^6/N^2$, $\rho = 997\ kg/m^3$, $\mu = 8.9\ 10^{-4}\ Pa\cdot s$, and $f = 0.62\ Hz$

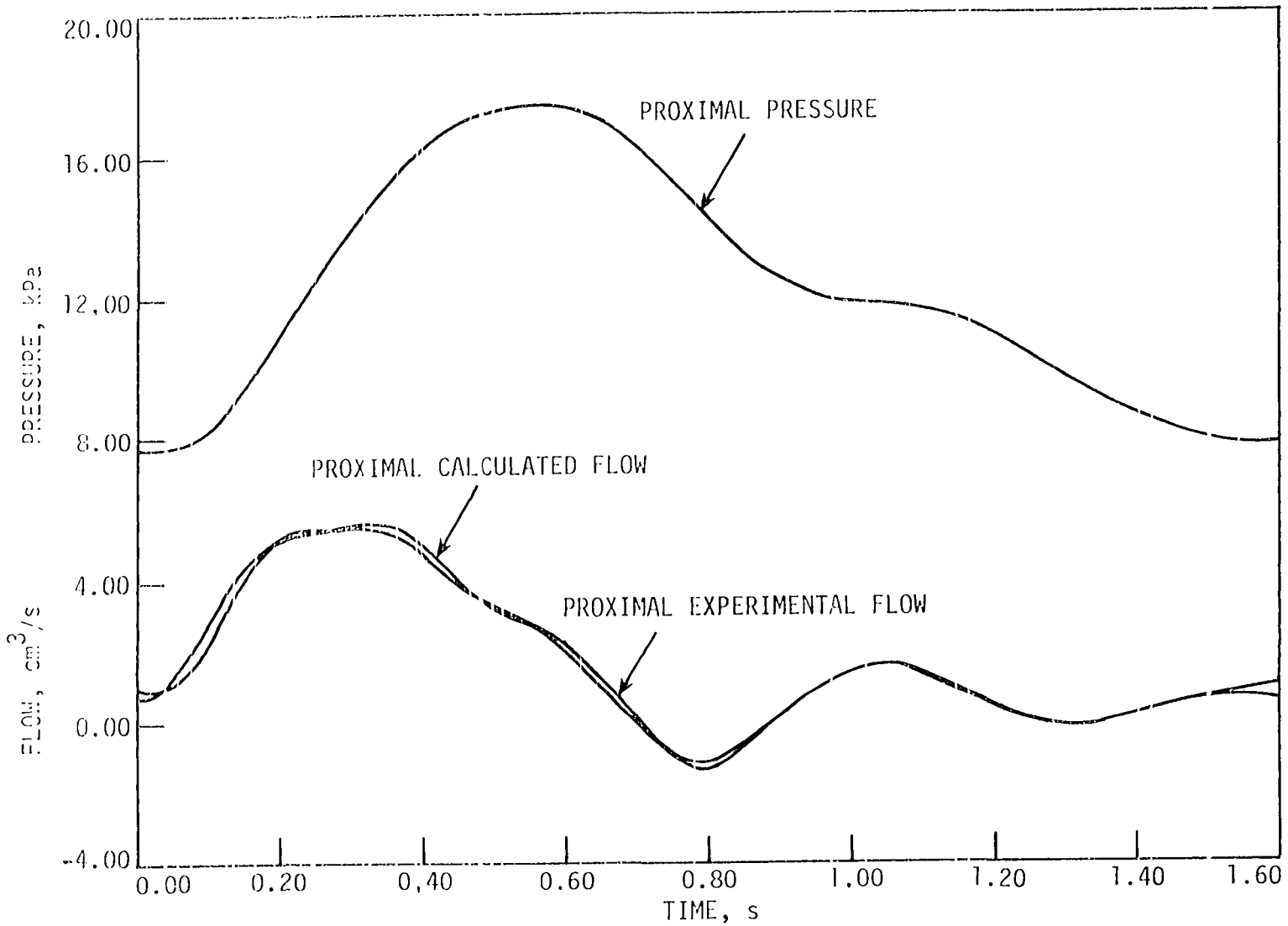
20.00
16.00
12.00
8.00
4.00
0.00
-4.00
PRESSURE, kPa
FLOW, cm3/s
PROXIMAL PRESSURE
PROXIMAL CALCULATED FLOW
PROXIMAL EXPERIMENTAL FLOW
0.00
0.20
0.40
0.60
0.80
1.00
1.20
1.40
1.60
TIME, s

for the nonlinear model, the same experimental data were reconstructed from the first ten harmonics (Figure 5).

Satisfactory results were obtained under all sets of boundary conditions except the one that was specified by proximal and distal pressures (P-P). For the sets (Q-Z) and (P-Q), the agreement between the calculated and the experimental waveforms was similar to that obtained for the set (P-Z) in Figure 4. Good agreement between the predicted and experimental pressures was also obtained for the boundary conditions (Q-Q), as illustrated in Figure 6. However, it was noted that for these boundary conditions, the solution may become unstable if there is a discrepancy between the means of the input proximal and distal flows. Even a small difference, which may result from small measurement error, was sufficient to cause instability in the predicted waveform. This result is to be expected since a difference between the mean flows is a violation of the continuity equation.

Predicted flow waveforms were also obtained for the boundary conditions (P-P). However, as previously noted, the results were not satisfactory because the predicted waveform was shifted considerably from the mean of the corresponding experimental curve. It is believed that this shift is due primarily to small experimental errors in the measured differences between the proximal and distal pressures. The differences between proximal and distal pressures is generally very small compared with the pressures themselves and these differences are within the range of experimental errors.

Figure 6. Comparison of proximal pressure predicted from the linear model with measured pressure. Flow-flow boundary conditions with parameters: $A_0 = 3.5\times10^{-5}m^2$, $C_0 = 3.1\times10^{-10}m^4/N$, $\rho = 997\ kg/m^3$, $\mu = 8.9\times10^{-4}$ Pa·s. amd f = 0.62 Hz

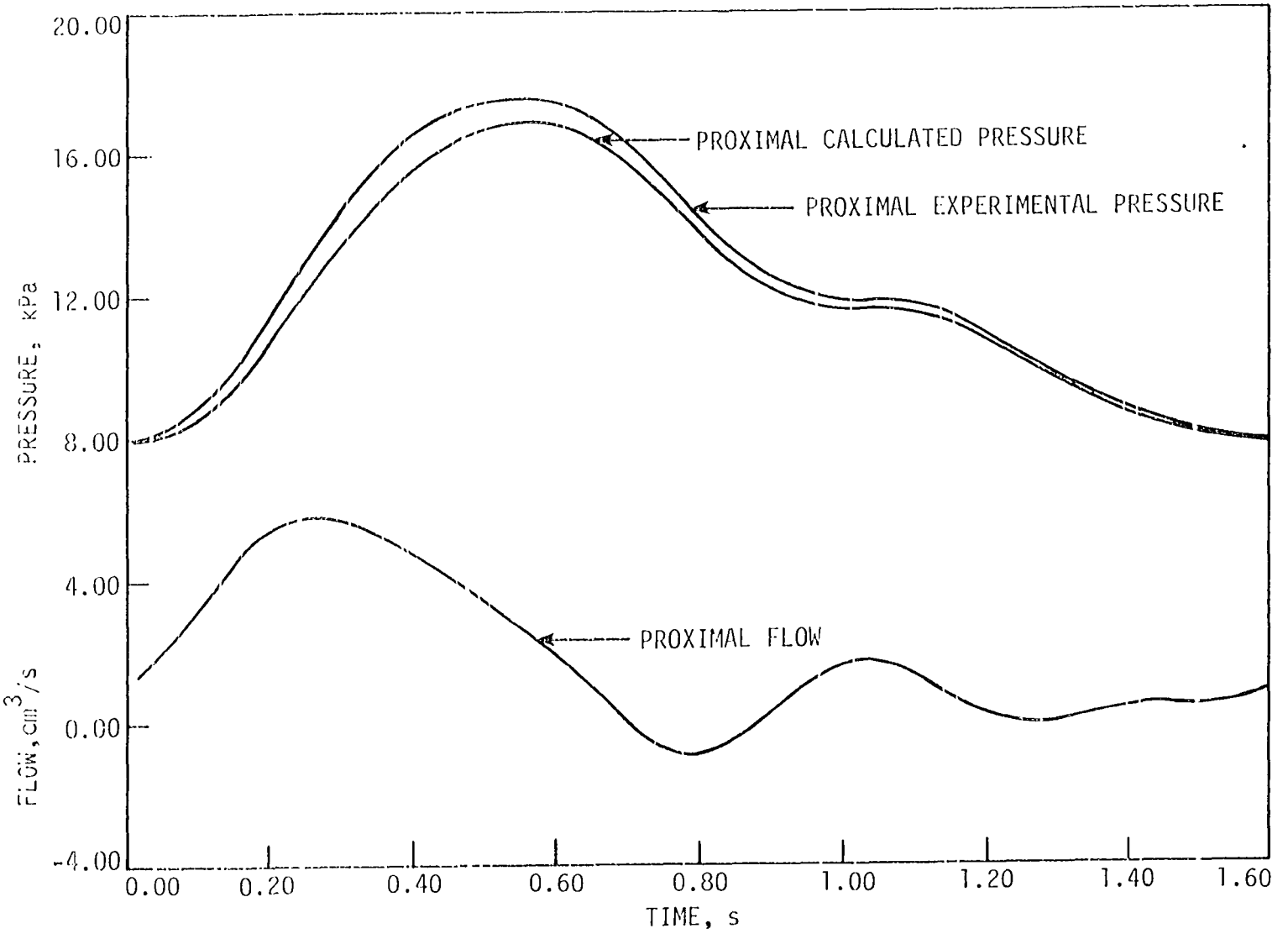
20.00
16.00
12.00
8.00
4.00
0.00
-4.00
PRESSURE, kPa
FLOW, cm³/s
PROXIMAL CALCULATED PRESSURE
PROXIMAL EXPERIMENTAL PRESSURE
PROXIMAL FLOW
0.00
0.20
0.40
0.60
0.80
1.00
1.20
1.40
1.60
TIME, s

Solutions were also obtained for a variety of frequencies of oscillation. The corresponding frequencies are given in Table 1, and these values are typical of those frequencies found in the cardiovascular system. It was found that over the range of frequencies used for the experiments, the model was equally applicable with no significant changes in the quality of the predicted waveform due to changes in frequency. Results for the highest frequency studied (1.49 Hz) are shown in Figure 7.

With the establishment of a valid model, the sensitivity of the predicted solution to different parameters could be investigated. In Figure 8, the effect of varying the radius on the flow waveform is demonstrated. It is clear from this plot that the solution is not highly sensitive to the vessel radius. In general, it was found that neither the flow nor the pressure waveforms are sensitive to changes in radius regardless of the boundary conditions used, or the location along the tube in which the waves are predicted.

Figure 9 shows pressure and flow waveforms which are calculated at different locations along the tube. The pressure waveforms at the five locations all fall essentially on the same curve (proximal pressure used as boundary condition), and individual curves cannot be distinguished on the scale used in the figure. Although the pressure reduction along the tube is very small, flow wave changes substantially between the proximal and distal ends of the tube. The damping of the flow waveform with axial location depends on the compliance of the tube, and it increases with an increase in compliance. The intensity of the pressure and waveforms at a specified location are also sensitive to a varying compliance. Figure 10

Figure 7. Comparison of proximal flow predicted from the linear model with measured flow. Pressure-peripheral resistance boundary conditions with parameters: $A_0 = 3.50\times10^{-5}m^2$, $C_0 = 3.1\times10^{-10}m^4/N$, $\rho = 997\ kg/m^3$, $\mu = 8.9\times10^{-4}\ Pa\cdot s$, and $f = 1.49\ Hz$

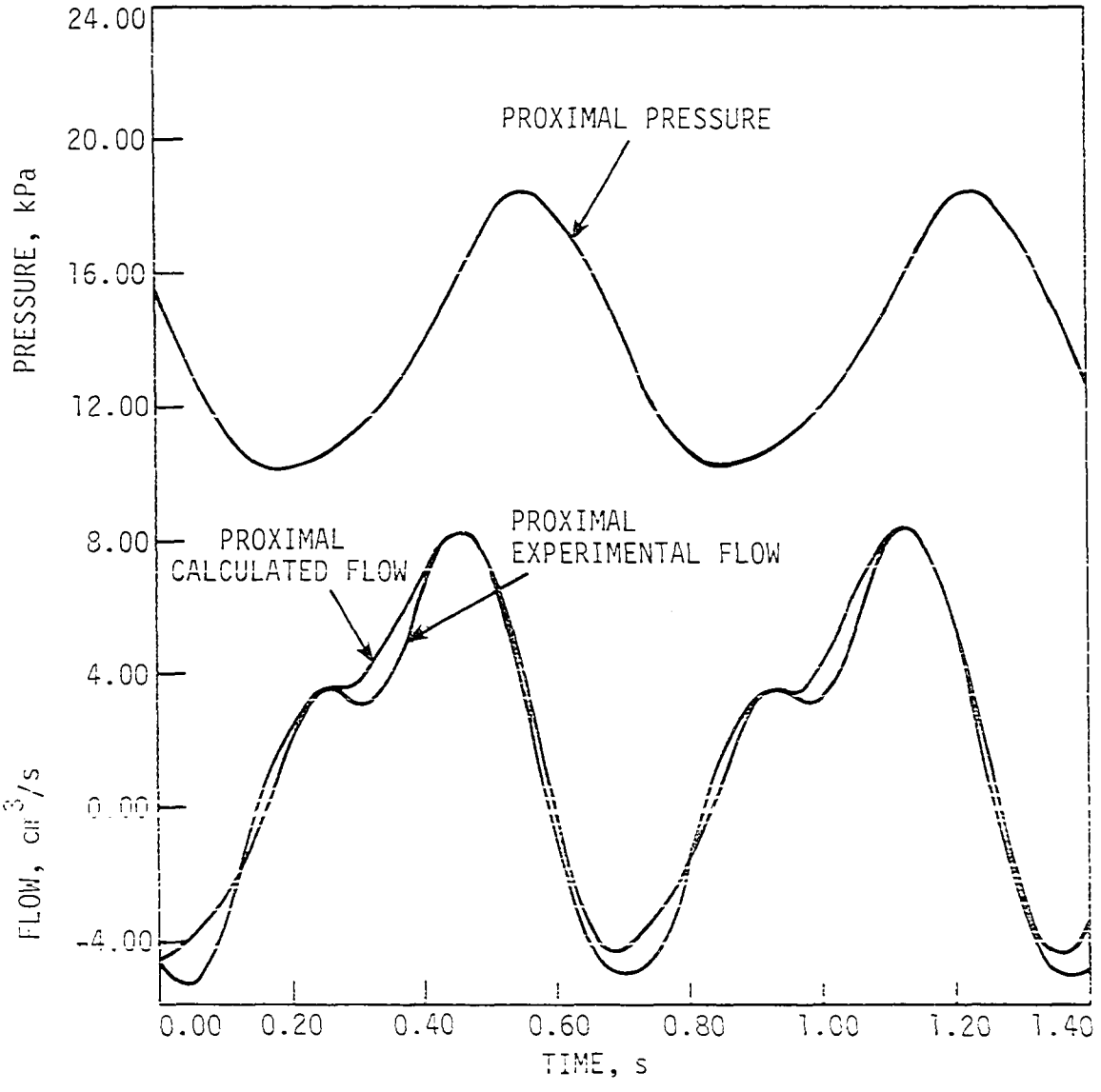
24.00
20.00
16.00
12.00
8.00
4.00
0.00
-4.00
PRESSURE, kPa
FLOW, cm³/s
PROXIMAL PRESSURE
PROXIMAL CALCULATED FLOW
PROXIMAL EXPERIMENTAL FLOW
0.00
0.20
0.40
0.60
0.80
1.00
1.20
1.40
TIME, s

Figure 8. Sensitivity of flow waveforms to changes in vessel radius; waveforms were evaluated at the proximal end of the tube

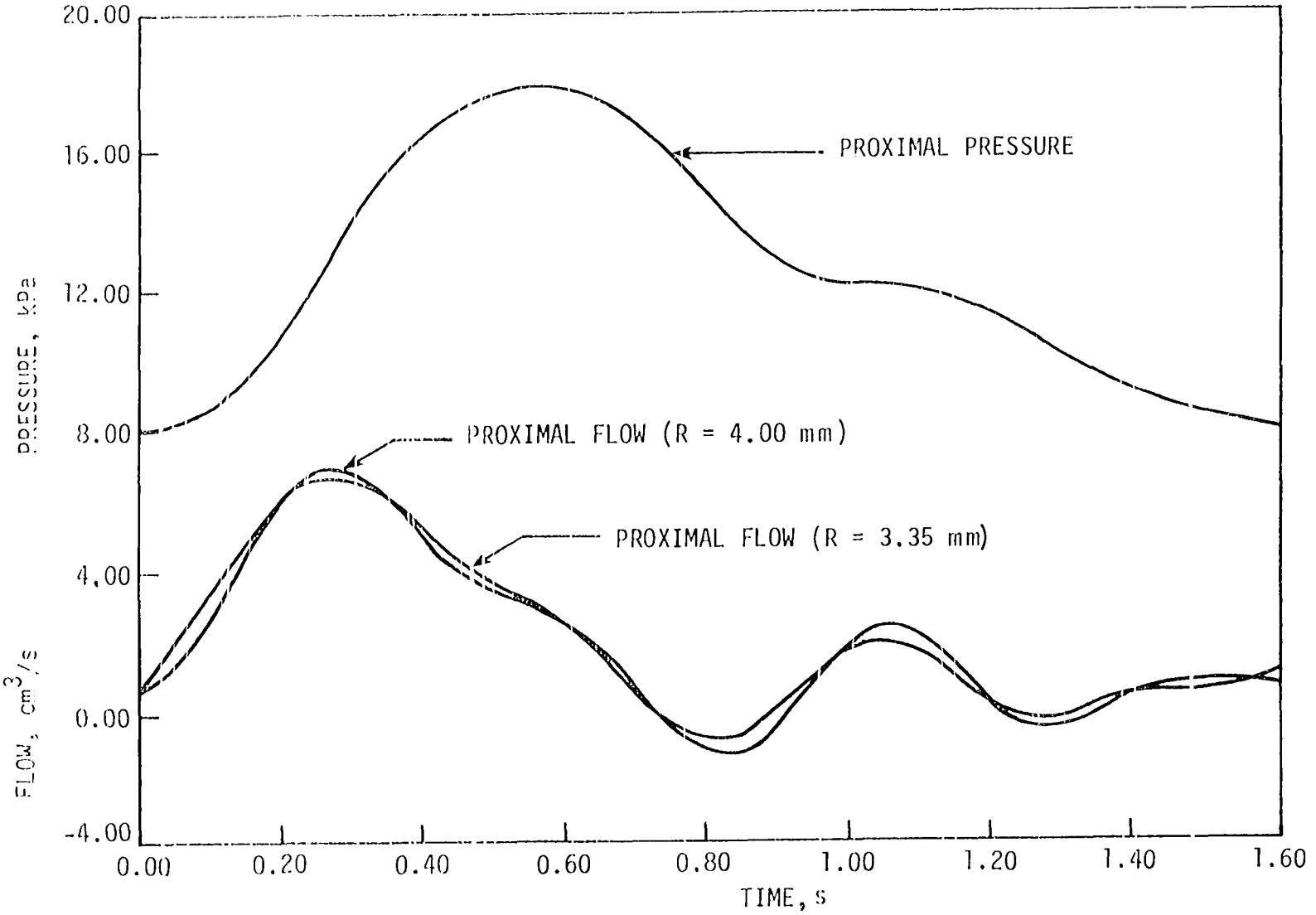
20.00
16.00
12.00
8.00
4.00
0.00
-4.00
PRESSURE, kPa
FLOW, cm³/s
PROXIMAL PRESSURE
PROXIMAL FLOW (R = 4.00 mm)
PROXIMAL FLOW (R = 3.35 mm)
0.00
0.20
0.40
0.60
0.80
1.00
1.20
1.40
1.60
TIME, s

Figure 9. Flow waveforms calculated at different locations along the tube

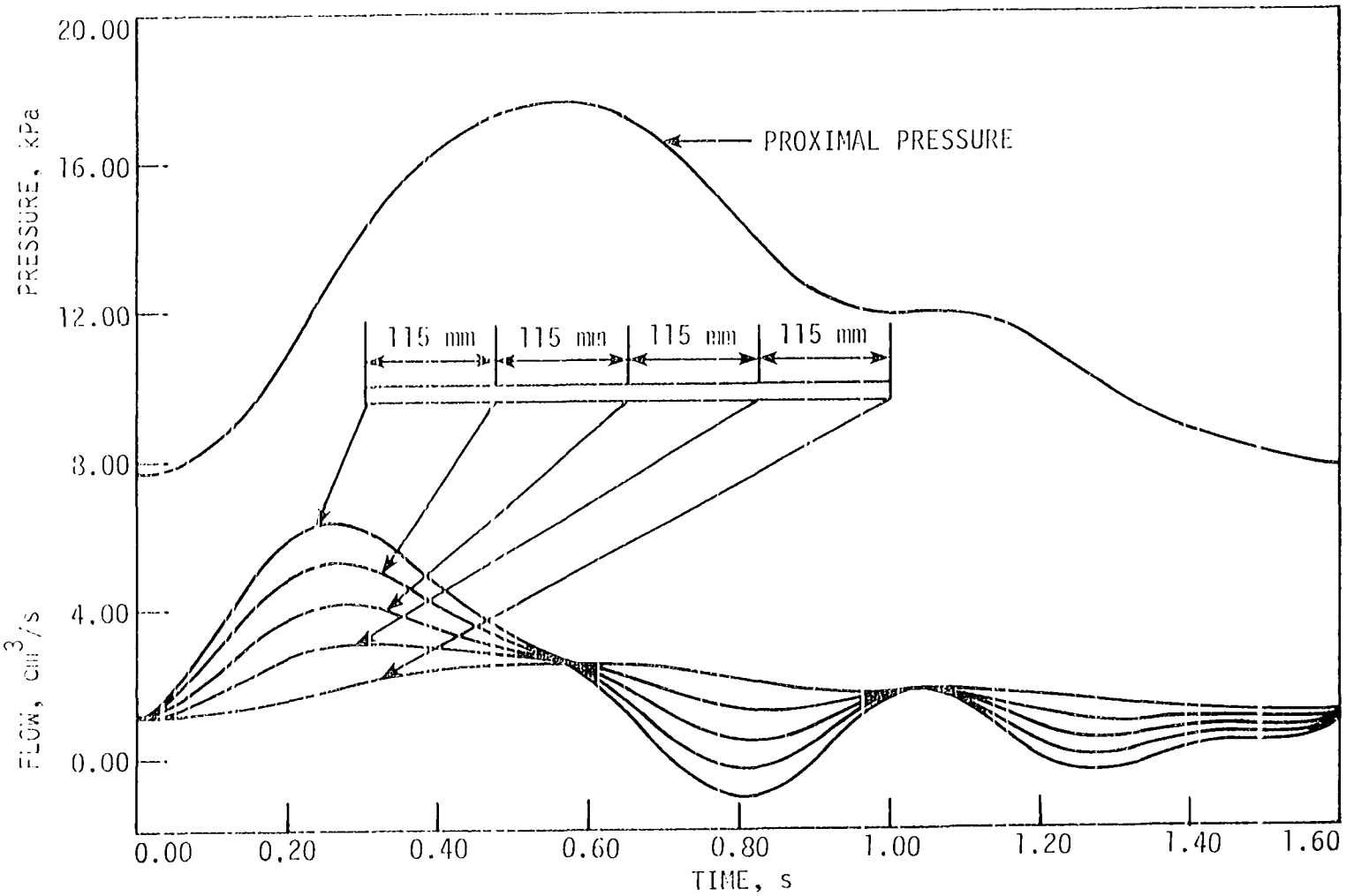
20.00
16.00
12.00
8.00
4.00
0.00
PRESSURE, kPa
FLOW, cm³/s
PROXIMAL PRESSURE
115 mm
115 mm
115 mm
115 mm
0.00
0.20
0.40
0.60
0.80
1.00
1.20
1.40
1.60
TIME, s

Figure 10. Sensitivity of flow waveforms to changes in vessel compliance; waveforms were evaluated at the proximal end of the tube

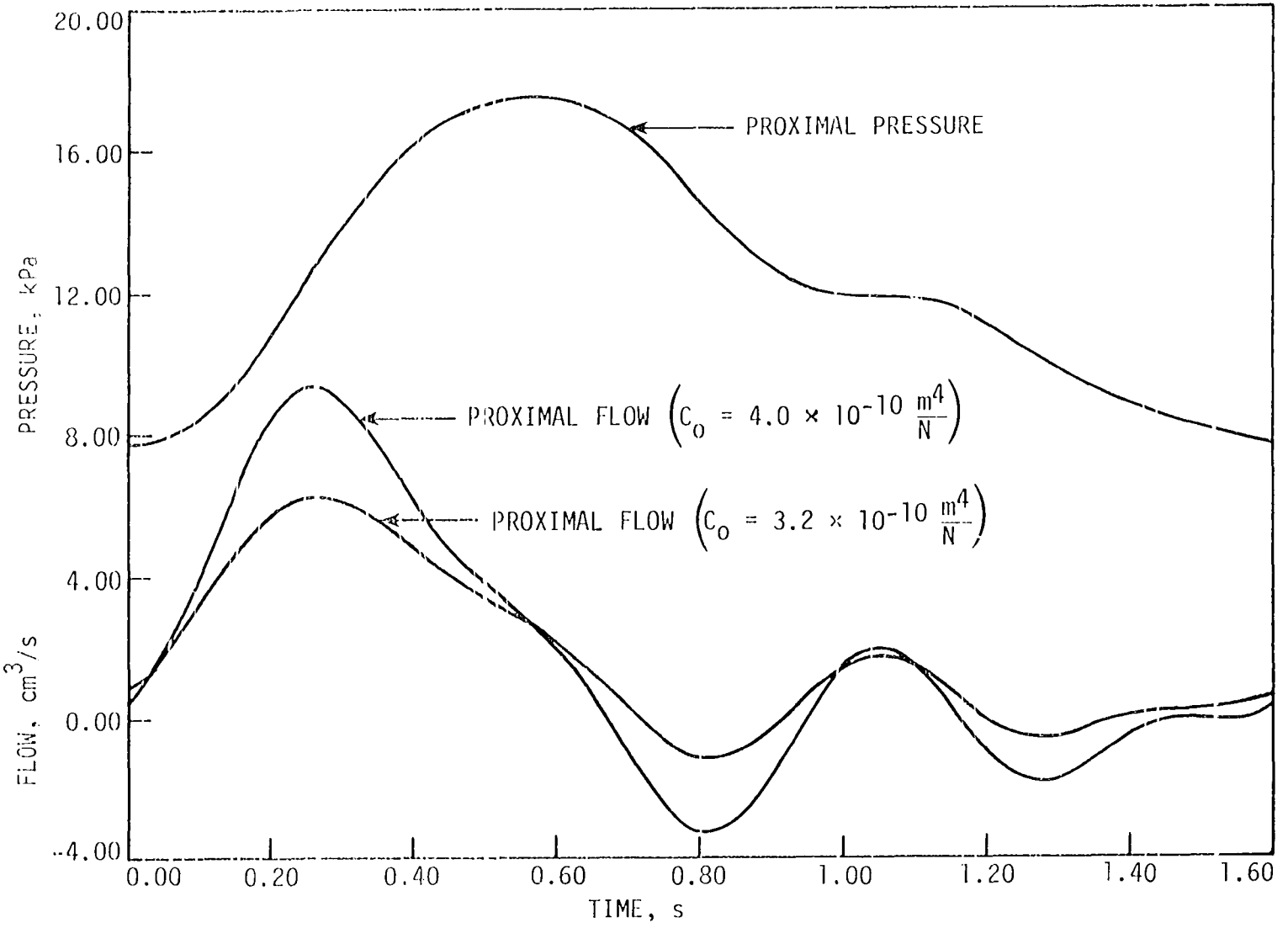
20.00
16.00
12.00
8.00
4.00
0.00
-4.00
PRESSURE, kPa
FLOW, cm³/s
PROXIMAL PRESSURE
PROXIMAL FLOW ($C_o = 4.0 \times 10^{-10} \frac{m^4}{N}$)
PROXIMAL FLOW ($C_o = 3.2 \times 10^{-10} \frac{m^4}{N}$)
0.00
0.20
0.40
0.60
0.80
1.00
1.20
1.40
1.60
TIME, s

indicates a marked elevation in the intensity of the flow wave due to an increase in compliance. It was observed, however, that the sensitivity to compliance of either the pressure or flow waveforms depends on the specified boundary conditions, and the location of the waveforms. In the case of boundary conditions (p-Z), the flow is most sensitive at the proximal end where it is not bounded, but this sensitivity is reduced towards the distal end where changes in flow are partially restricted by the fixed relationship between flow, pressure, and resistance. In contrast, the pressure is not very sensitive to the compliance near the proximal end where it is fixed by the input proximal pressure, but its sensitivity increases towards the distal end.

SUMMARY

In this study, a finite-element model for a simple hydraulic system involving a pulsatile flow in a straight flexible tube was developed. Two versions of the model, one involving a linear equation of state (constant compliance) and the other involving a nonlinear equation of state (non-constant compliance), were investigated. It was possible to assess the validity of the model through a comparison of the predicted flow and pressure waveforms and corresponding measured waveforms obtained from the hydraulic system. The results indicate that the linear model can be used to satisfactorily predict both flow and pressure waveforms for a variety of boundary conditions and a variety of frequencies of oscillation. In addition, it was demonstrated that the agreement between the predicted and experimental results can be improved through the use of a nonlinear model which utilizes a nonlinear equation of state relating the vessel cross-sectional area and pressure. With the establishment of a valid model, it is possible to study the sensitivity of flow and pressure waveform to the various system parameters, such as vessel compliance and radius.

Although other numerical techniques have been used to solve this type of flow problem (method of characteristics and method of finite difference), it is believed that the finite-element method represents a very useful approach to this type of problem. The true potential and value of the finite-element model lies in its potential applicability to more complex problems where the model can be readily expanded to include other factors such as vessel taper, partial obstruction (stenosis) of the tube,

branching, and more realistic models for the peripheral resistance. The use of the model to study flow through stenoses is illustrated in Part II of this paper.

REFERENCES

1. Cox, R. H. "Comparison of linearized wave propagation models for arterial blood flow analysis." J. Biomechanics, 2 (1969), 251-265.

2. Womersley, J. R. "Oscillatory flow in arteries. The constrained elastic tube as a model of arterial flow in pulse transmission." Phys. Med. Biol., 2 (1958), 178-187.

3. Skalak, R. and T. C. Stathis. "A porous tapered elastic tube model of a vascular bed." In Biomechanics, Y. C. Fung, Ed. New York: A.S.M.E., 1966.

4. Fox, E. A. and E. Saibel. "A formulation of the problem of flow through tubes." Proc. 4th International Congress on Rheology. New York: John Wiley and Sons, Inc., 1965.

5. Skalak, R. "Synthesis of a complete circulation." In Cardiovascular Fluid Dynamics, vol. 2, D. H. Bergel, Ed. New York: Academic Press, 1972.

6. Raines, J. K., M. Y. Jaffrin and A. H. Shapiro. "A computer simulation of arterial dynamics in the human leg." J. Biomechanics, 7 (1974), 77-91.

7. Streeter, V. L., W. F. Keitzer and D. F. Bohr. "Pulsatile pressure and flow through distensible vessels." Circ. Res., 13 (1963), 3-20.

8. Westerhof, N., F. Bosman, C. J. DeVries and A. Noordergraaf. "Analog studies of the human systemic arterial tree." J. Biomechanics, 2 (1969), 121-143.

9. Desai, C. S. and J. F. Abel. Introduction to the Finite Element Method. New York: Van Nostrand Reinhold Company, 1972.

10. Segerlind, L. J. Applied Finite Element Analysis. New York: John Wiley and Sons, Inc., 1976.

A FINITE-ELEMENT SIMULATION OF PULSATILE FLOW IN FLEXIBLE TUBES--PART-II. FLOW IN AN OBSTRUCTED TUBE

Elkana Rooz
Donald F. Young
Thomas R. Rogge

From the Department of Engineering Science and Mechanics and the Biomedical Engineering Program, Iowa State University, Ames, IA 50011

Supported by the Engineering Research Institute of Iowa State University.

ABSTRACT

The finite-element model for pulsatile flow in a flexible unobstructed tube described in Part-I is expanded to include a stenosis. The applicability of the model is checked by comparing predicted flow and pressure waveforms with corresponding experimental results obtained from in vitro measurements on a mechanical system. The laboratory model includes a pulsating pump, a latex tube partially obstructed by a hollowed, cylindrical rigid plug, and a peripheral resistance. Good agreement is found between predicted and experimental flow and pressure waveforms.

NOMENCLATURE

A_0	Average cross-sectional area at average pressure p_0
A_i	Minimum cross-sectional area of stenosis
[A*]	Coefficient matrix of linear terms in a model
a	Half length of an element
[B*]	Coefficient matrix of nonlinear terms in a model
b	Half of time step
C_0', C_1'	Coefficients of compliance
D	Vessel diameter
D_1	Minimum diameter of stenosis
f	frequency of waveform
K_t, K_u, K_v	coefficients
L_s	Length of the stenosis
[N]	Shape function matrix
p	Pressure
p_i	Nodal pressure
p_u	Pressure upstream of stenosis
P_s	Pressure downstream of stenosis
Q	Flow
q_i	Nodal flow
Q_s	Flow in the obstructed area
r	Dimensionless axial length coordinate
s	Dimensionless time coordinate
t	Time
x	Axial length coordinate

$\{\delta^*\}$	Vector of unknowns
μ	Fluid viscosity
ρ	Fluid density

INTRODUCTION

Arterial disease is one of the leading causes of deaths in the United States and much research has been directed toward the study of this disease. One important aspect of this form of circulatory disorder is the development of a localized narrowing in an artery (stenosis) due to atherosclerotic involvement. Once a stenosis has formed, the blood flow through the diseased artery can be significantly altered, and fluid-mechanical effects associated with flow through stenoses have been the subject of a number of previous studies.

One of the most serious consequences of a partial occlusion due to a stenotic obstruction in a major artery is the reduction of blood flow to the vascular beds supplied by the artery. In previous investigations concerned with the nature of this reduction [1,2], it was observed that in most cases, there were no significant effects on blood flow until the percent reduction of the obstructed cross-sectional area (percent stenosis) reached a critical value of approximately 60%. Several investigators (see for example, Young [3]) have demonstrated, however, that reduction of mean blood flow cannot be simply characterized by the percent stenosis, since the blood flow also depends on other factors such as peripheral resistance and collateral flow. Thus, normal mean flow under resting conditions can be maintained in a severely obstructed vessel due to a compensatory decrease in the peripheral resistance.

Other studies have shown that a developing stenosis progressively alters the shape of the pressure and flow waveforms both upstream and downstream of the obstruction [4]. These changes are produced by wave

reflection from the discontinuity (stenosis) in the elastic vessel. Farrar et al. [5] in a study of stenosis effects on the Fourier harmonic moduli of the pressure and flow waveforms demonstrated that gradual changes in the severity of the stenosis produced increases in the values of the harmonic moduli of the proximal pressure waveform, and decreases in the harmonic moduli of the proximal flow and distal pressure and flow waveforms. Furthermore, it also was observed that the zero harmonic modulus (mean flows or pressures) were less sensitive to a developing obstruction than the higher harmonic moduli. For example, at 70% stenosis, the zero harmonic modulus of the proximal flow was approximately 85% of the baseline (0% stenosis) zero harmonic modulus and the first, second, and third harmonic moduli were approximately 75%, 65%, and 55%, respectively, of the baseline values.

These past experimental studies indicate that changes in pressure and flow waveforms may represent relatively sensitive indicators of the presence of a stenosis. However, the various factors which affect the waveforms are not clearly understood, and they are difficult to evaluate from in vivo experiments due to a lack of control of the physiologic variables. An alternate approach is a computer simulation of pulsatile flow in a flexible tube containing a stenosis which would allow for a systematic study of these factors. Thus, the purpose of the present study is to develop a finite-element model for pulsatile flow in an obstructed flexible tube, and to use this model to investigate quantitatively the effects of a developing stenosis on the flow waveform. To accomplish this, the model for the unobstructed tube in Part-I is expanded to include a relationship

between flow and pressure drop across a stenotic obstruction at a specified location along the tube. The model is validated by comparing calculated waveforms with corresponding experimental results. The experimental results were obtained from *in vitro* measurements of pulsatile flow in a latex flexible tube which is partially occluded by a rigid plug in the shape of a hollowed cylinder.

GOVERNING EQUATIONS

Unobstructed Tube

The model for pulsatile flow in an unobstructed flexible tube in Part-I was developed on the basis of one-dimensional flow equations. The model includes two equations which are derived from considerations of conservation of mass and momentum and a third equation of state which relates the cross-sectional area with the pressure.

The momentum equation was linearized by assuming that: (a) the convective acceleration term is negligible; (b) the friction term is proportional to the flow rate (approximated by Poiseuille flow); and (c) the changes in cross-sectional area due to changes in pressure are negligible compared with the cross-sectional area itself and, therefore, the varying cross-sectional area in the coefficients of the momentum equations can be approximated by a constant average cross-sectional area, A_0.

The dependence of the cross-sectional area on the pressure (equation of state) is approximated by a quadratic polynomial equation with the coefficients of this equation obtained by direct measurements of the changes in cross-sectional area with pressure. The basic equations of this model are

$$\frac{\partial Q}{\partial x} + C_0' \frac{\partial p}{\partial t} + C_1' p \frac{\partial p}{\partial t} = 0 \tag{1}$$

$$\frac{\rho}{A_0} \frac{\partial Q}{\partial t} + \frac{\partial p}{\partial x} + \frac{8\pi\mu}{A_0^2} Q = 0 \tag{2}$$

where equation (1) is obtained by combining the continuity equation with

the equation of state and equation (2) is the linearized momentum equation.

Stenosis

The instantaneous pressure drop across a stenosis under pulsatile flow conditions depends on three elements. The first is energy dissipation due to viscous flow in the obstructed area. The second is the energy loss associated with nonlinear entrance effects and with the highly disturbed flow in the expansion region downstream of the stenosis. The third is the energy required to accelerate the blood over the length of the obstruction.

On the basis of an extensive series of *in vitro* measurements utilizing models of arterial stenosis, Young and Tsai [6] proposed that the instantaneous pressure drop could be calculated from the following equation

$$\Delta p = \frac{4K_v\mu}{\pi D^3} Q_s + \frac{8K_t}{\pi^2 D^4} \left(\frac{A_0}{A_1} - 1\right)^2 |Q_s| Q_s + \frac{K_u \rho L}{\pi D^2} \frac{dQ_s}{dt} \tag{3}$$

where the first term in the equation represents viscous losses, the second term represents highly nonlinear losses due to entrance-exit effects, and the third term represents the pressure differential required for accelerating flow.

The coefficients K_v, K_t and K_u are empirical quantities and generally they depend on the stenosis geometry and the frequency parameter $\alpha = D\sqrt{\omega/\nu}/2$. The coefficients K_t and K_u appear to be only slightly dependent on stenosis geometry and the frequency parameter, and they can be adequately approximated by constants with values of 1.52 and 1.2, respec-

tively [7,6]. For the range of alpha parameter commonly found in the circulatory system, the pulsatile flow is frequently approximated by a quasi-steady flow, and consequently the viscous term can be approximated by results obtained in steady-flow. For a steady flow, the coefficient K_v has been determined empirically for a stenosis geometry in the shape of a hollowed cylindrical plug with stenosis length L_s by the equation [7]

$$K_v = 32 \frac{L_a}{D} \left(\frac{A_0}{A_1}\right)^2 \tag{4}$$

with

$$L_a = 0.83L_s + 1.64D_1 \tag{5}$$

where L_a represents a modified stenosis length which absorbs the effects of a nonparabolic velocity profile at the entrance and exit of the tube.

Comparisons of the pressure drops estimated by equation (3) with those obtained from <u>in vivo</u> experiments [8] show reasonable agreement and support the applicability of the equation.

NUMERICAL METHOD

Unobstructed Tube

As discussed in Part-I, for the unobstructed tube equations, the finite-element method was applied on both time and axial length coordinates to reduce the system of partial differential equations (1) and (2) to a system of algebraic equations. The method is briefly reviewed here. A linear isoparametric quadrilateral element was considered. For this element, the shape function is

$$[N] = \begin{bmatrix} N^1 \\ N^2 \end{bmatrix} = \begin{bmatrix} N_1, 0, N_2, 0, N_3, 0, N_4, 0 \\ 0, N_1, 0, N_2, 0, N_3, 0, N_4 \end{bmatrix}$$

and

$$N_i = \frac{1}{4}(1 + rr_i)(1 + ss_i),\ r_i = \pm 1,\ s_i = \pm 1,\ i = 1, 2, 3, 4$$

where r and s are the dimensionless coordinates corresponding to axial length and time, respectively. Within the element, the pressure and flow representation is

$$\begin{Bmatrix} p \\ Q \end{Bmatrix} = [N]\{\delta\}_e$$

and

$$\{\delta\}_e = [p_1, q_1, p_2, \ldots, p_4, q_4]^T$$

where p_1, q_1, etc., are the nodal values of pressures and flows.

The pressure flow representation is substituted into equations (1) and (2), and the Galerkin method is employed to obtain the element equations.

The finite-element scheme propagates in marching time increments where in each time increment, the solution for one line of elements

representing the total tube length is obtained (see Figure 1, Part-I). Therefore, for the global system of equations, there are assembled a set of elements along the axial length axis and one time increment along the time axis. For each time increment, k, half of the number of unknown nodal pressures and flows (initial conditions) are specified by the solution of the previous time increment, k-1. Substitution of these initial conditions into the global matrix equation yields a reduced matrix equation where only half of the original number of nodal pressures and flows are unknowns. The reduced matrix equation is

$$[A^*]\{\delta^*\} + [B^*]\{\delta^*\} = \{f^*\} \tag{6}$$

where $[A^*]$ and $[B^*]$ are coefficient matrices corresponding to the linear and nonlinear terms in the model equations, respectively. The vector of the unknowns is

$$\{\delta^*\} = [p_2, q_2, p_4, \cdots, q_{2n-2}, p_{2n}, q_{2n}]^T$$

and $\{f^*\}$ is a force vector that emerges from the substitution of the initial conditions.

In addition, two boundary conditions are required to completely define the problem. The first is prescribed by the pressure at the inlet of the tube (proximal pressure) and the second by the flow at the outlet of the tube (distal flow), or alternatively by the peripheral resistance. The treatment of a boundary condition, prescribed by either pressure or flow, is to substitute its value into the reduced matrix equation. For a boundary condition specified by the peripheral resistance, the last equation of the system represented by equation (6) is replaced by an algebraic equation which relates the distal pressure and flow with the resistance.

Stenosis

For a stenosis specified in element m, the unobstructed tube element equations corresponding to the stenosis element are removed from the global system yielding two independent systems of equations that correspond to the two tube sections upstream and downstream of the stenosis. In the obstructed element, the governing equations are

$$P_{2m}^{k} - P_{2m+2}^{k} = \frac{4K_v}{\pi D^3} Q_{2m}^{k} + \frac{8K_t \rho}{\pi^2 D^4} \left(\frac{A_0}{A_1} - 1\right)^2 |Q_{2m}^{k}| Q_{2m}^{k} + \frac{K_u \rho L}{\pi D^2} \frac{Q_{2m}^{k} - Q_{2m}^{k-1}}{\Delta t} \tag{7}$$

and

$$Q_{2m}^{k} = Q_{2m+2}^{k} \tag{8}$$

where Δt is the time increment.

Solution to the algebraic system of equations of the obstructed tube is obtained by employing an iterative procedure which involves a combination of a modified bisection method and the method of solution for the unobstructed tube described in Part-I. Further details of the iterative procedure are available in reference [9].

EXPERIMENTAL MODEL AND INPUT PARAMETERS

A complete description and a schematic of the basic flow system is given in Part-I. The main three elements of the mechanical system are the pulsatile pump, a section of flexible (latex) tubing, and a peripheral resistance. To simulate the stenosis, a rigid plug in the shape of a hollowed cylinder made from Plexiglas was inserted into the tube. Pressures and flows at the inlet and outlet of the tube were recorded simultaneously. The experimental data were sampled, digitized, and calibrated with a minicomputer (PDP8/e) and subsequently transferred to a high speed digital computer (Itel AS6). For each measured waveform, Fourier harmonic moduli were obtained, and subsequently, the Fourier series representation of the experimental waveforms was used for input boundary conditions in the numerical solution, and for data for evaluation of the model.

Input Parameters

Through all the experiments, physiological saline with density of 997 kg/m^3 and viscosity of 8.9×10^{-4} Pa·s was used. The coefficients of the compliance C_0^* and C_1^* were obtained from direct measurements of the variation of the cross-sectional area with pressure (see input parameters, Part-I) and their values were found to equal 1.0 m^4/N and 1.4 m^6/N^2, respectively. Two hollowed plugs both with outer diameters of 6.36 mm and lengths of 10 mm were used. These plugs had inner diameters of 2.00 mm and 3.18 mm corresponding to 75.0% and 90.1% stenosis, respectively.

RESULTS AND DISCUSSION

Validation of the Mathematical Model

To validate the finite-element model, computer solutions for different conditions which included different frequencies of oscillation, percent stenosis, and locations of stenosis were compared with measured results. Proximal pressure and distal flow were measured and used as boundary conditions in the computer model. In addition, specified values of fluid density, viscosity, vessel compliance, mean vessel radius, length of vessel, outer and inner diameters of the obstructing plug and length of the plug were used as input parameters. Examples of comparisons of the calculated and measured waveforms for the proximal flow and distal pressure are shown in Figures 1 through 4. In general, it was found that the model satisfactorily predicts both the pressure and flow waveforms and it is equally applicable for the range of the different condition (frequency of oscillation, percent stenosis and location of stenosis) used. It was therefore assumed that this model could be used to study the effect of a developing stenosis on the pulsatile waveforms.

Stenosis Effects on the Flow Waveform

To approximately simulate the flow conditions which may be found in the circulation, a set of boundary conditions which included proximal pressure and distal resistance was used. One driving proximal pressure was used for all the calculations. The same normal mean flow for different stenosis severities was maintained by altering the value of the

Figure 1. Comparison of predicted proximal flow and distal pressure predicted with measured flow and pressure for an obstructed tube; the reduction of lumen area due to stenosis is 90.1%, the stenosis is located midway between the proximal and distal ends of the tube, and f = 1.03 Hz

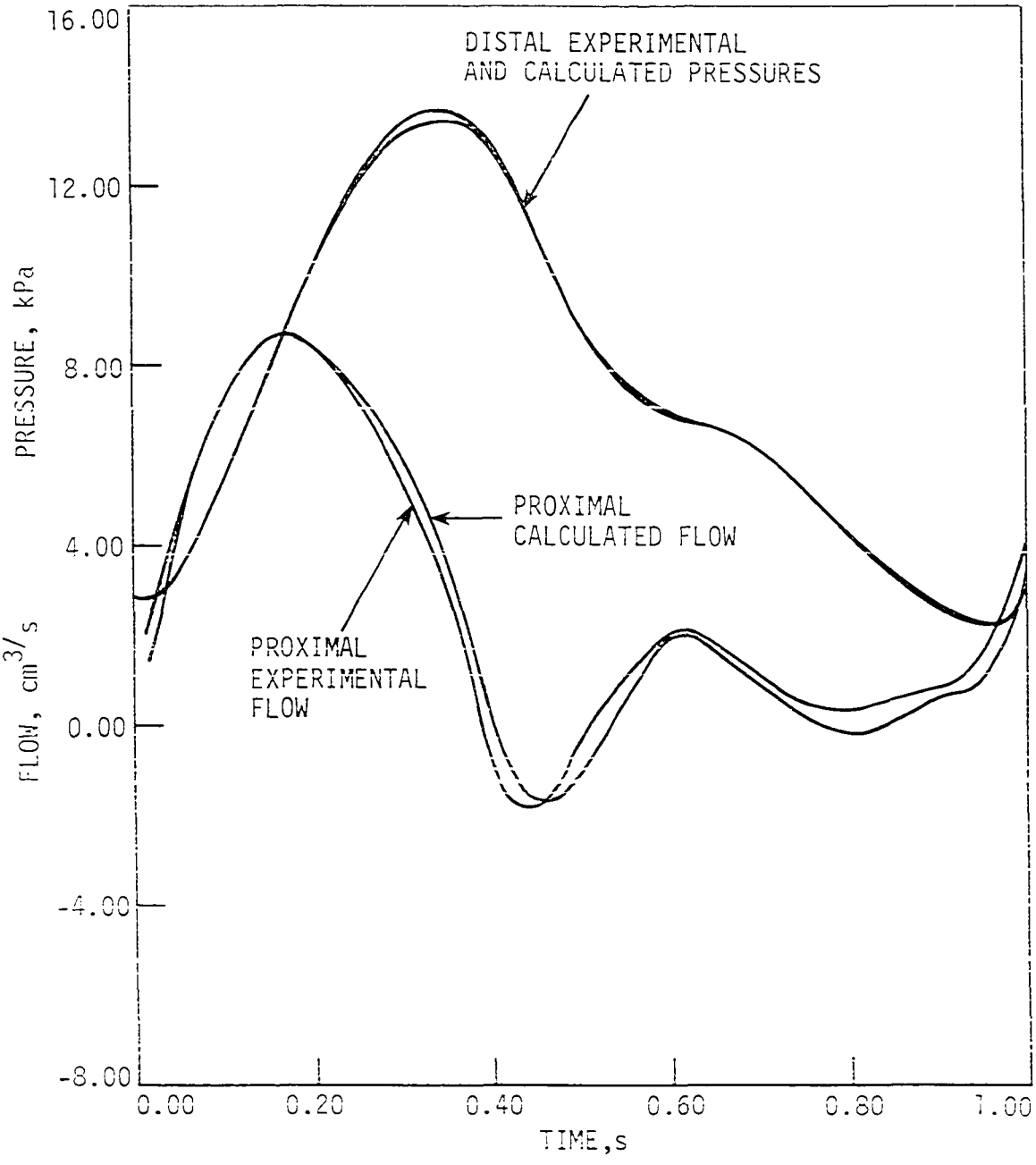
16.00
12.00
8.00
4.00
0.00
-4.00
-8.00
PRESSURE, kPa
FLOW, cm3/s
DISTAL EXPERIMENTAL
AND CALCULATED PRESSURES
PROXIMAL
CALCULATED FLOW
PROXIMAL
EXPERIMENTAL
FLOW
0.00
0.20
0.40
0.60
0.80
1.00
TIME,s

Figure 2. Comparison of predicted proximal flow and distal pressure predicted with measured flow and pressure for an obstructed tube; the reduction of lumen area due to stenosis is 90.1%, the stenosis is located midway between the proximal and distal ends of the tube, and f = 0.66 Hz

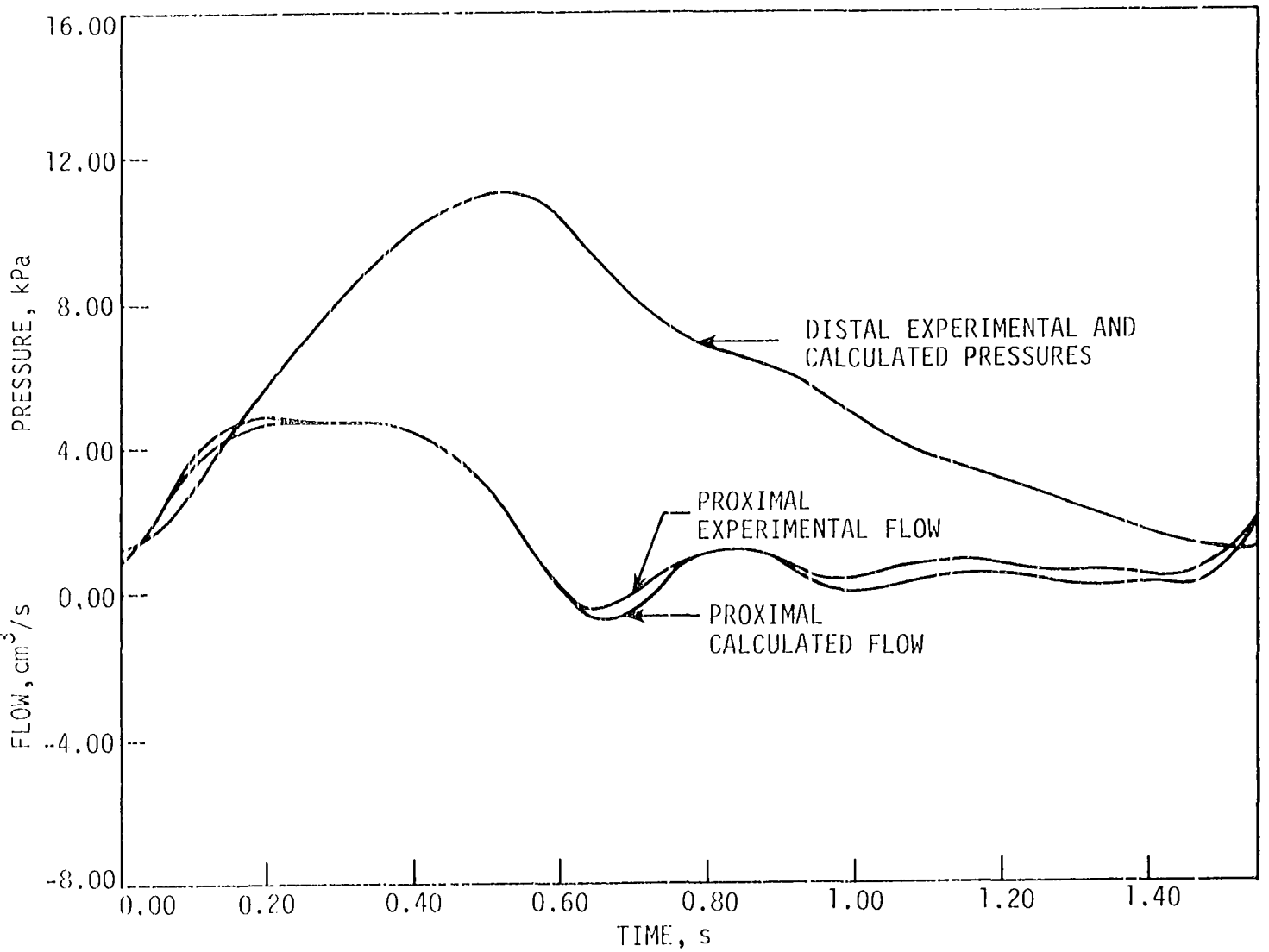
16.00
12.00
8.00
4.00
0.00
-4.00
-8.00
PRESSURE, kPa
FLOW, cm³/s
DISTAL EXPERIMENTAL AND
CALCULATED PRESSURES
PROXIMAL
EXPERIMENTAL FLOW
PROXIMAL
CALCULATED FLOW
0.00
0.20
0.40
0.60
0.80
1.00
1.20
1.40
TIME, s

Figure 3. Comparison of predicted proximal flow and distal pressure with measured flow and pressure for an obstructed tube; the reduction of lumen area due to stenosis is 75%, the stenosis is located midway between the proximal and distal ends of the tube, and f = 0.74 Hz

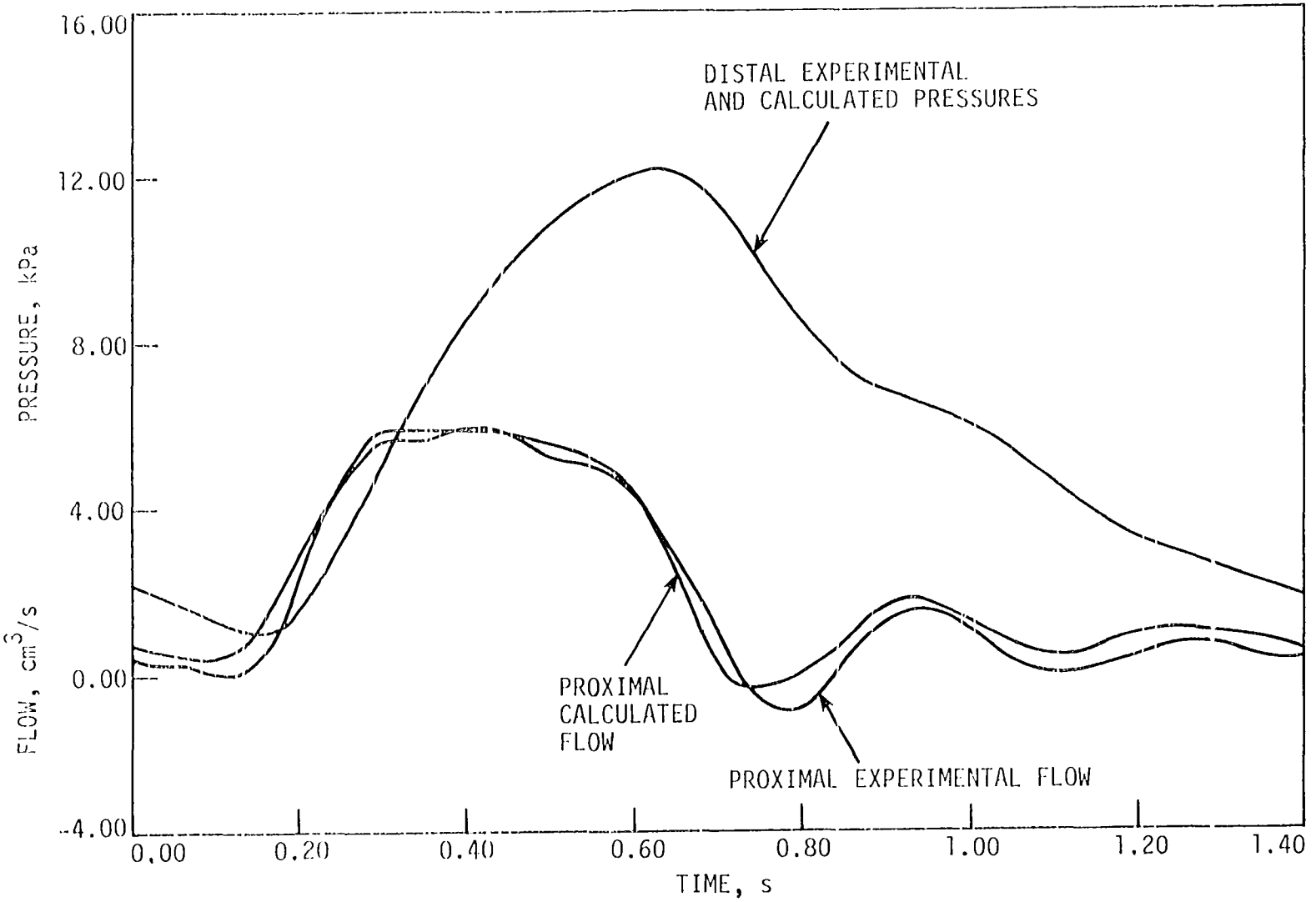
16.00
12.00
8.00
4.00
0.00
-4.00
PRESSURE, kPa
FLOW, cm³/s
DISTAL EXPERIMENTAL
AND CALCULATED PRESSURES
PROXIMAL
CALCULATED
FLOW
PROXIMAL EXPERIMENTAL FLOW
0.00
0.20
0.40
0.60
0.80
1.00
1.20
1.40
TIME, s

Figure 4. Comparison of predicted proximal flow and distal pressure with measured flow and pressure for an obstructed tube; the reduction of lumen area due to stenosis is 75%, the stenosis is located quarter tube length from the proximal end, and f = 1.03 Hz

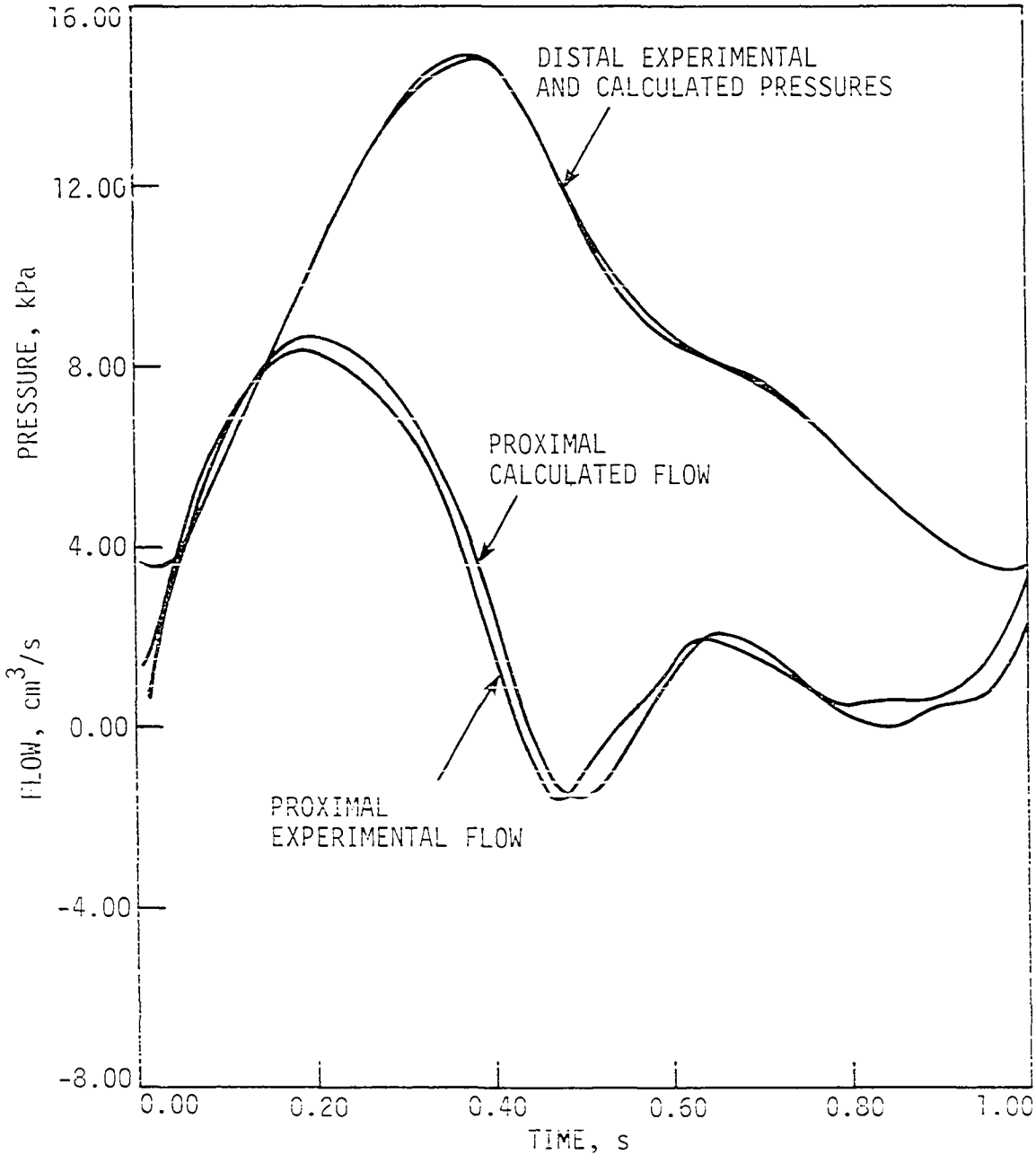
16.00
12.00
8.00
4.00
0.00
-4.00
-8.00
PRESSURE, kPa
FLOW, cm3/s
DISTAL EXPERIMENTAL
AND CALCULATED PRESSURES
PROXIMAL
CALCULATED FLOW
PROXIMAL
EXPERIMENTAL FLOW
0.00
0.20
0.40
0.60
0.80
1.00
TIME, s

peripheral resistance. Thus, for example, for an increase in percent stenosis which was simultaneously followed by a decrease of mean flow, the peripheral resistance was decreased until the normal mean flow was achieved. In one case, a lower limit for the peripheral resistance was assumed and a solution with a reduced mean flow was obtained.

Effects of a gradually increasing stenosis (50%, 75%, 85% and 95%) under constant mean flow conditions are illustrated in Figure 5. It is clear that an increasing stenosis is progressively depressing the pulsatility of the flow waveform. This observation is consistent with in vivo experimental results obtained by other investigators [4,5]. Figure 5 also illustrates a flow waveform with reduced mean flow for 95% stenosis. In this case, the mean flow was reduced by approximately 34%. Comparison of this waveform and the one with the normal mean flow, also for 95% stenosis, indicates that the pulsatility (ratio of peak to mean flow) of the reduced mean flow waveform is less sensitive to stenosis changes.

The Fourier harmonic moduli of the waveforms illustrated in Figure 5 were obtained as a quantitative measure of waveform changes. The percentage reduction of the first five harmonic moduli with respect to the corresponding moduli which were obtained under conditions of 0% stenosis are given in Figure 6. Higher harmonics were not considered since their magnitude was small and fell within the range of calculation errors. As it would be expected, the magnitudes of the first four zero harmonics (mean flows) are approximately equal. Slight differences are due to the

Figure 5. Effects of a developing stenosis on the proximal flow waveform; four waveforms have the same normal mean flow; the fifth waveform has a mean flow reduced by approximately 35%

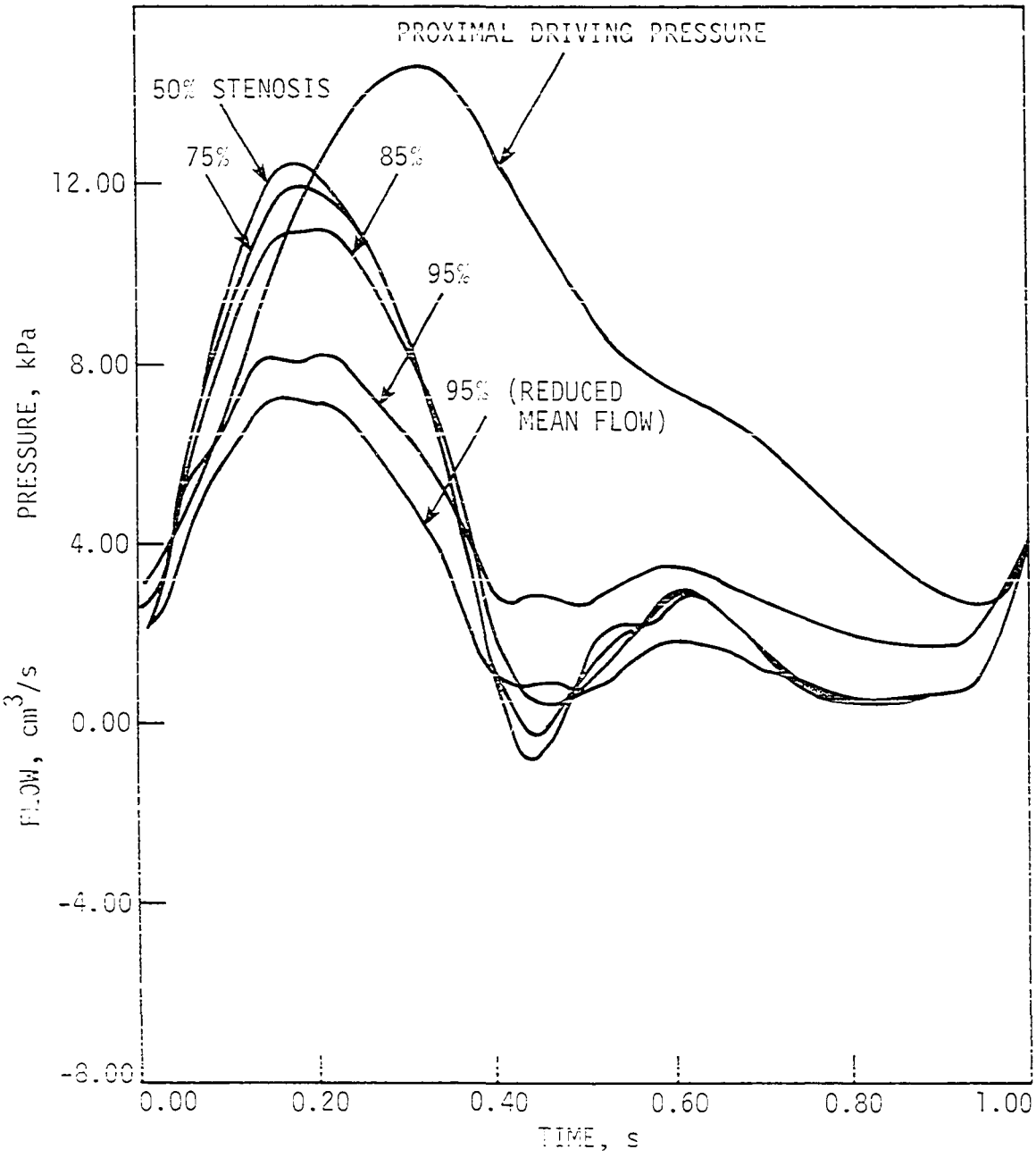
PROXIMAL DRIVING PRESSURE
50% STENOSIS
75%
85%
95%
95% (REDUCED MEAN FLOW)
12.00
8.00
4.00
0.00
-4.00
-8.00
PRESSURE, kPa
FLOW, cm³/s
0.00
0.20
0.40
0.60
0.80
1.00
TIME, s

Figure 6. Percent reduction of the Fourier harmonic moduli obtained from the waveforms illustrated in Figure 5; the reduction is measured with respect to harmonic moduli obtained from a corresponding unobstructed waveform

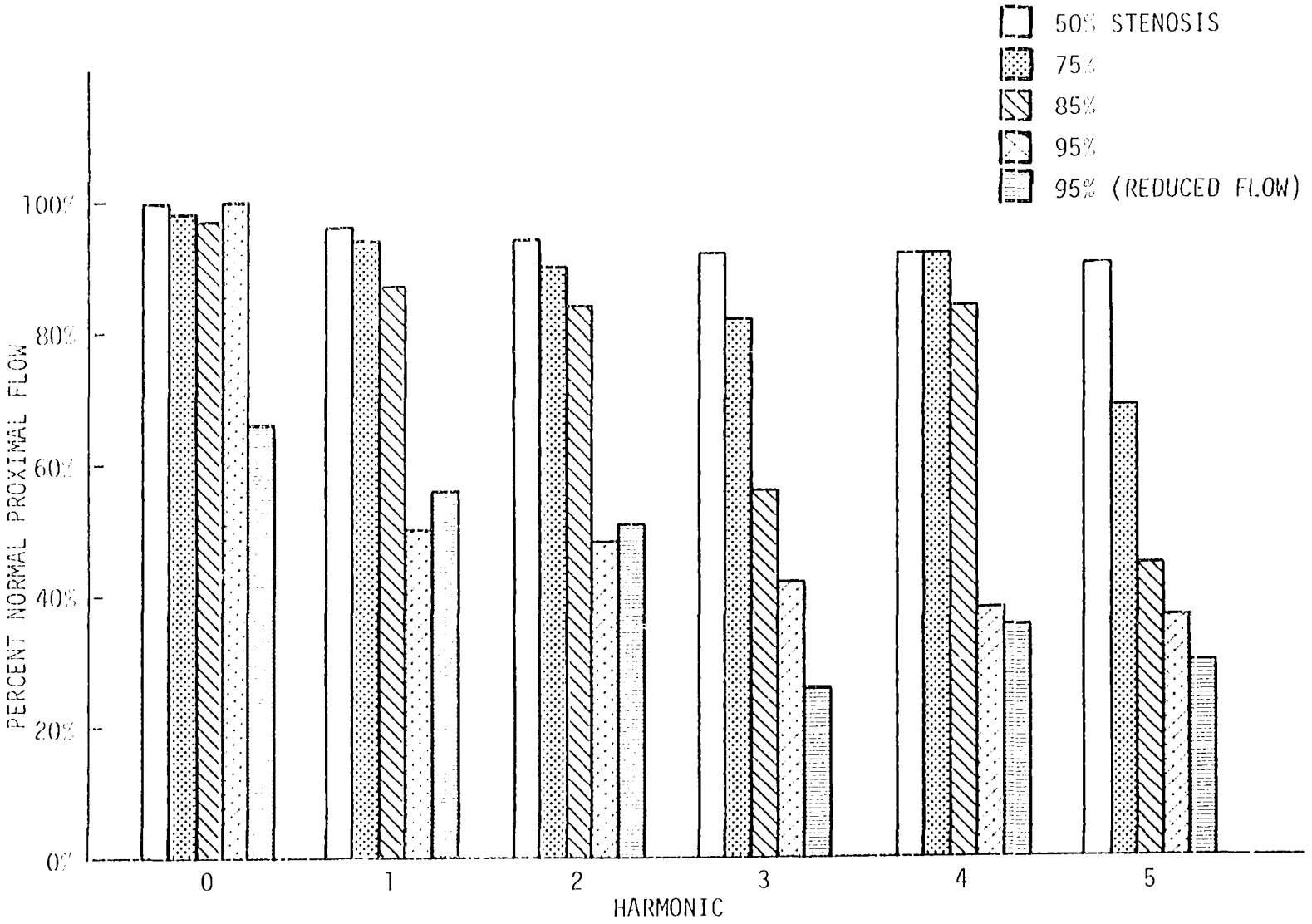
50% STENOSIS
75%
85%
95%
95% (REDUCED FLOW)
100%
80%
60%
40%
20%
0%
PERCENT NORMAL PROXIMAL FLOW
0
1
2
3
4
5
HARMONIC

numerical scheme used to adjust the peripheral resistance to maintain a constant mean flow. In general, it is noted that the magnitudes of the nonzero harmonic moduli are reduced by an increasing percent stenosis. The reduction for a given percent stenosis, however, is not necessarily a uniform reduction with increasing frequency. Thus, for example, harmonics one, two and four are not highly sensitive to changes of mild or moderate stenoses (below 80%) but are highly sensitive to changes in severe stenosis, whereas harmonics three and five demonstrate more uniform attenuation over the range of 50% to 100% stenosis. Figure 6 also illustrates the reduction of harmonics that were obtained under conditions of reduced mean flow. For this 95% stenosis, the reduction of the zero harmonic modulus is 34%, whereas the reductions of the five nonzero harmonic moduli are 44%, 49%, 74%, 64%, and 70%, respectively. Thus, even with reduced mean flow, there are still significant changes in the higher harmonics.

In general, the effect of a stenosis on the harmonic moduli, as illustrated in Figure 6, exhibits trends which are similar to those reported in previous studies [4,5]. Quantitatively, however, these effects show different frequency dependence on the stenosis geometry. For example, the finding of Farrar et al. [5] indicates that the third and the fourth harmonics were more sensitive to the stenosis changes than the first harmonic, whereas the results from the computer model indicate similar sensitivity for the first, second, and fourth harmonics. It is believed that these differences arise primarily from the different conditions under which the waveforms were obtained. In Farrar et al., the flow waveforms were obtained in the vicinity of the proximal end of the

stenosis, whereas in the present study, the flow waveforms were calculated at the inlet of the tube far from the stenosis. The significance of the location at which the waveform is recorded is demonstrated in Figure 7. This figure illustrates simultaneous flow waves calculated at different sites along the tube. It is clear that the various waveforms and consequently their harmonic composition are different. Another factor, in addition to the stenosis geometry and stenosis location that may influence the flow waveform, is the nature of the resistance distal of the stenosis. In this study, the simplest model for this resistance was used, i.e., a "pure" resistance. In the circulatory system, however, the distal resistance may include elements which are produced by other factors such as compliance of the peripheral vascular bed. It is clear that the effect of a stenosis on the flow waveform cannot be simply characterized by the stenosis geometry, and that a full understanding of this complex problem involves examination of all the various factors mentioned above.

Figure 7. Simultaneous flow waveforms predicted at different locations along the tube

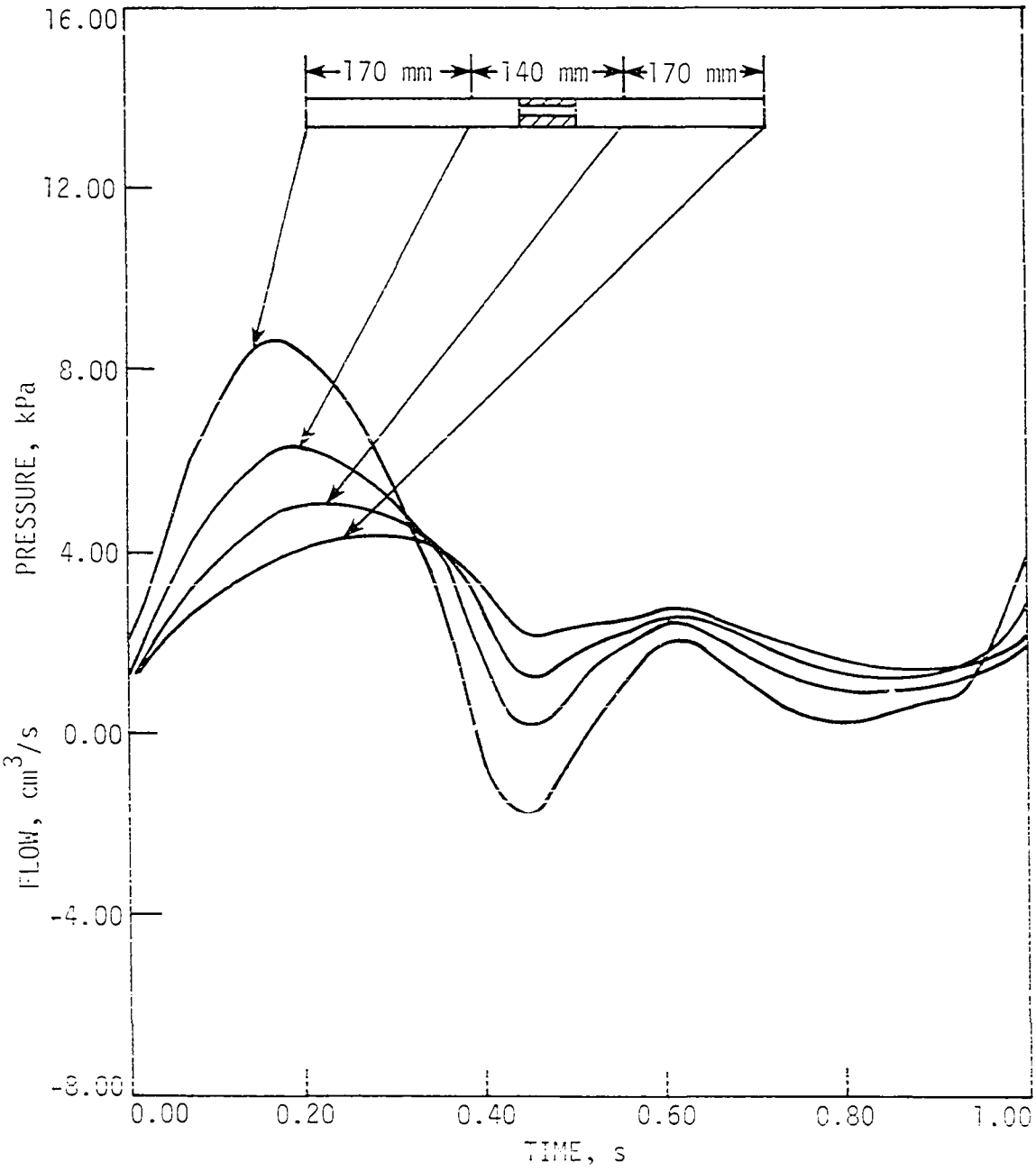
16.00
12.00
8.00
4.00
0.00
-4.00
-8.00
PRESSURE, kPa
FLOW, cm3/s
170 mm
140 mm
170 mm
0.00
0.20
0.40
0.60
0.80
1.00
TIME, s

SUMMARY

In this study, a finite-element model for pulsatile flow in obstructed flexible tube was developed. The model was checked by comparing calculated and experimental results, and was shown to give good agreement. The validated model was subsequently used to investigate certain effects of a developing stenosis on the flow waveform. These results, when compared with past *in vivo* studies, support the applicability of the model and provide useful information with regard to the various factors that influence this type of flow problems. It is believed that computer modeling of the type presented can prove to be useful in the study of the fluid-mechanical aspects of arterial disease.

REFERENCES

1. Shipley, R. E. and D. E. Gregg. "The effect of external constriction of a blood vessel on blood flow." American Journal of Physiology, 141 (1944), 289-296.

2. May, A. G., L. Van de Berg, J. A. DeWeese and C. G. Rob. "Critical arterial stenosis." Surgery, 54 (1963), 250-259.

3. Young, D. F. "Fluid mechanics of arterial stenosis." ASME Journal of Biomechanical Engineering, 101 (1979), 157-175.

4. Newman, D. L., R. K. Walesby and N. L. R. Bowden. "Haemodynamic effects of acute experimental aortic coarctation in the dog." Circulation Research, 36 (1975), 165-172.

5. Farrar, D. J., H. D. Green and D. W. Peterson. "Noninvasively and invasively measured pulsatile haemodynamics with graded arterial stenosis." Cardiovascular Research, 13 (1979), 45-57.

6. Young, D. F. and F. Y. Tsai. "Flow characteristics in models of arterial stenoses-II. Unsteady flow." Journal of Biomechanics, 6 (1973), 547-559.

7. Seely, B. D. and D. F. Young. "Effect of geometry on pressure losses across models of arterial stenoses." Journal of Biomechanics, 9 (1976), 439-448.

8. Young, D. F., N. R. Cholvin and A. C. Roth. "Pressure drop across artificial induced stenoses in the femoral arteries of dogs." Circulation Research, 36 (1975), 735-743.

9. Rooz, E. "Pulsatile flow in flexible tubes." Ph.D. dissertation, Iowa State University, Ames, Iowa, 1980.

SUMMARY

The fluid-mechanical aspects of blood flow in both normal and occluded large arteries were studied using the following steps:

1. Finite-element models for pulsatile flow in both unobstructed and obstructed tubes were developed.
2. The applicability of these models was checked by comparing predicted solutions for pressures and flows with experimental results.
3. The experimental results were obtained from *in vitro* measurements on an experimental laboratory system.
4. The validated models were used to study the various factors that influence the pulsating flow.

The principal results obtained in this study are as follows:

1. The assumptions made in the development of the mathematical models are reasonable since the models satisfactorily predict the pressure and flow waveforms.
2. The finite-element method provides a powerful numerical technique for the study of pulsatile flow problems.
3. The pressure and flow waveforms in the unobstructed tube are not sensitive to changes in tube radius but they are sensitive to changes in vessel compliance.
4. In the obstructed tube, a developing stenosis progressively alters the shape, and consequently the harmonic composition of the flow waveform. The general trend is a decreasing waveform pulsatility with increasing percent stenosis.

It is believed that computer modeling of the type presented can be useful in the study of blood flow problems related to the circulatory system.

It is suggested that future research expand the present models to include other elements of the circulatory system which may play a significant role in the study of pulsating blood flow in arteries. These elements would include:

1. Tapering of the tube in which the average cross-sectional area is function of the axial length coordinate. In this case, the effect of the convective acceleration may not be negligible.
2. A more realistic representation of the peripheral bed resistance to include the effect of the bed compliance.
3. Branches emanating from the main artery which carry either collateral flow into the artery or distribute flow to the various peripheral vascular beds.

ACKNOWLEDGMENTS

I am indebted to my major professors, Dr. D. F. Young and Dr. T. R. Rogge, for their always helpful guidance throughout my Ph.D. program, for their encouragement during my research, and for editing this thesis. I must also thank Dr. R. C. Seagrave, Dr. N. R. Cholvin, Dr. G. A. Nariboly, and Dr. T. H. Okiishi for serving on my committee and for editing this thesis.

APPENDIX A

This details the finite-element method used to obtain element equations for the unobstructed tube. The element used in this study is shown below.

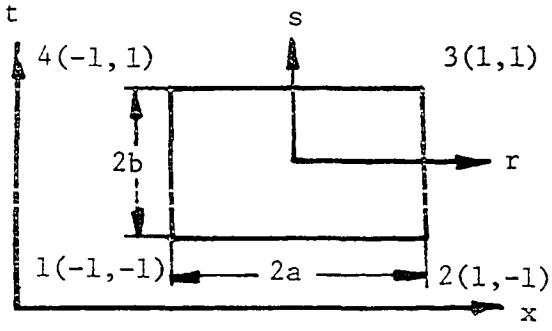

The partial differential equations of the unobstructed tube with the nonlinear equation of state are

$$\frac{\partial Q}{\partial x} + C_0' \frac{\partial p}{\partial t} + C_1' p \frac{\partial p}{\partial t} = 0 \tag{A1}$$

$$\frac{\partial p}{\partial x} + L \frac{\partial Q}{\partial t} + RQ = 0 \tag{A2}$$

The linear isoparametric shape functions for the quadrilateral element are

$$[N] = \frac{1}{4}[(1 - r)(1 - s),\ (1 + r)(1 - s),\ (1 + r)(1 + s),\ (1 - r)(1 + s)] \tag{A3}$$

where r and s are dimensionless coordinates corresponding to the axial length, x, and the time, t, coordinates respectively. The relations between r, s, x and t are

$$r = \frac{x - x_0}{a} \tag{A4}$$

$$s = \frac{t - t_0}{b} \tag{A5}$$

where (x_0, t_0) = center of rectangle. And,

$$\frac{dr}{dx} = \frac{1}{a} \tag{A6}$$

$$\frac{ds}{dt} = \frac{1}{b} \tag{A7}$$

$$dx\ dt = a\ b\ dr\ ds \tag{A8}$$

Within the element, the pressure and flow are approximated by

$$p = [N]\{p_n\} \tag{A9}$$

and

$$Q = [N]\{q_n\} \tag{A10}$$

where $\{p_n\}$ and $\{q_n\}$ are the nodal pressures and flows given as

$$\{p_n\} = [p_1, p_2, p_3, p_4]^T \tag{A11}$$

$$\{q_n\} = [q_1, q_2, q_3, q_4]^T \tag{A12}$$

Therefore,

$$\frac{\partial p}{\partial t} = \frac{\partial p}{\partial s}\ \frac{ds}{dt} = \frac{1}{b}\frac{\partial [N]}{\partial s}\{p_n\} = \frac{1}{4b}[-(1-r), -(1+r), (1+r), (1-r)]\{p_n\} \tag{A13}$$

$$\frac{\partial p}{\partial x} = \frac{\partial p}{\partial r}\frac{dr}{dx} = \frac{1}{a}\frac{\partial [N]}{\partial r}\{p_n\} = \frac{1}{4a}[-(1-s), (1-s), (1+s), -(1+s)]\{p_n\} \tag{A14}$$

$$\frac{\partial Q}{\partial t} = \frac{\partial Q}{\partial s}\frac{ds}{dt} = \frac{1}{b}\frac{\partial [N]}{\partial s}\{q_n\} = \frac{1}{4b}[-(1-r), -(1+r), (1+r), (1-r)]\{q_n\} \tag{A15}$$

and

$$\frac{\partial Q}{\partial x} = \frac{\partial Q}{\partial r}\frac{dr}{dx} = \frac{1}{a}\frac{\partial [N]}{\partial r}\{q_n\} = \frac{1}{4a}[-(1-s), (1-s), (1+s), -(1+s)]\{q_n\} \tag{A16}$$

The Galerkin method leads to

$$\int_A [N]^T\left(\frac{\partial Q}{\partial x} + C_0'\frac{\partial p}{\partial t} + C_1'p\frac{\partial p}{\partial t}\right)dA = 0 \tag{A17}$$

and

$$\int_A [N]^T \left(\frac{\partial p}{\partial x} + L\frac{\partial Q}{\partial t} + RQ\right) dA = 0 \tag{A18}$$

Substitution of equations (13), (14), (15), and (16) into equations (17) and (18) and performing the appropriate integration gives

$$\int_{-1}^{1}\int_{-1}^{1} [N]^T \frac{\partial Q}{\partial x}\, a\, b\, dr\, ds = \frac{b}{6}\begin{bmatrix} -2 & 2 & 1 & -1 \\ -2 & 2 & 1 & -1 \\ -1 & 1 & 2 & -2 \\ -1 & 1 & 2 & -2 \end{bmatrix} \{q_n\} \tag{A19}$$

$$\int_{-1}^{1}\int_{-1}^{1} [N]^T C_0' \frac{\partial p}{\partial t}\, a\, b\, dr\, ds = \frac{C_0' a}{6}\begin{bmatrix} -2 & -1 & 1 & 2 \\ -1 & -2 & 2 & 1 \\ -1 & -2 & 2 & 1 \\ -2 & -1 & 1 & 2 \end{bmatrix} \{p_n\} \tag{A20}$$

$$\int_{-1}^{1}\int_{-1}^{1} [N]^T \frac{\partial p}{\partial x}\, a\, b\, dr\, ds = \frac{b}{6}\begin{bmatrix} -2 & 2 & 1 & -1 \\ -2 & 2 & 1 & -1 \\ -1 & 1 & 2 & -2 \\ -1 & 1 & 2 & -2 \end{bmatrix} \{p_n\} \tag{A21}$$

$$\int_{-1}^{1}\int_{-1}^{1} L[N]^T \frac{\partial Q}{\partial t}\, a\, b\, dr\, ds = \frac{L\, a}{6}\begin{bmatrix} -2 & -1 & 1 & 2 \\ -1 & -2 & 2 & 1 \\ -1 & -2 & 2 & 1 \\ -2 & -1 & 1 & 2 \end{bmatrix} \{q_n\} \tag{A22}$$

$$\int_{-1}^{1}\int_{-1}^{1} R[N]^T Q\, a\, b\, dr\, ds = \frac{R\, a\, b}{9}\begin{bmatrix} 4 & 2 & 1 & 2 \\ 2 & 4 & 2 & 1 \\ 1 & 2 & 4 & 2 \\ 2 & 1 & 2 & 4 \end{bmatrix} \{q_n\} \tag{A23}$$

and

$$\int_{-1}^{1}\int_{-1}^{1} C_1'[N]^T\, p\,\frac{\partial p}{\partial t}\, a\, b\, dr\, ds = \frac{C_1'}{32b}\,[B]\{p_n\} \tag{A24}$$

where B is nonconstant coefficient matrix whose elements are

$$B_{11} = -4p_1 - 4/3p_2 + 1/3p_3 + p_4$$

$$B_{12} = -4/3p_1 - 4/3p_2 + 1/3p_3 + 1/3p_4$$

$$B_{13} = 1/3p_1 + 1/3p_2 + 2/3p_3 + 2p_4$$

$$B_{14} = -1/3p_1 - 1/3p_2 + 2/3p_3 + 2p_4$$

$$B_{21} = -4/3p_1 - 4/3p_2 + 1/3p_3 + 1/3p_4$$

$$B_{22} = -4/3p_1 - 4/3p_2 + 1/3p_3 + 1/3p_4$$

$$B_{23} = 1/3p_1 + p_2 + p_3 + 2/3p_4$$

$$B_{24} = 1/3p_1 + 1/3p_2 + 2/3p_3 + 2/3p_4$$

$$B_{31} = -2/3p_1 - 2/3p_2 - 1/3p_3 - 1/3p_4$$

$$B_{32} = -2/3p_1 - 2p_2 - p_3 - 1/3p_4$$

$$B_{33} = -1/3p_1 - p_2 + 4p_3 + 4/3p_4$$

$$B_{34} = -1/3p_1 - p_2 + 4/3p_3 + 4/3p_4$$

$$B_{41} = -2p_1 - 2/3p_2 - 1/3p_3 - p_4$$

$$B_{42} = -2/3p_1 - 2/3p_2 + 4/3p_3 - 4/3p_4$$

$$B_{43} = -1/3p_1 - 1/3p_2 + 4/3p_3 + 4/3p_4$$

$$B_{44} = -p_1 - 1/3p_2 + 4/3p_3 + 4p_4$$

The overall matrix equation for one element is

$$[A]_e\{\dot{\delta}\}_e + [B]_e\{\delta\}_e = 0 \tag{A25}$$

where

$$[A]_e = \begin{bmatrix} -6C_0'a & -6b & -3C_0'a & 6b & 3C_0'a & 3b & 6C_0'a & -3b \\ -6b & -6La+8Rab & 6b & -3La+4Rab & 3b & 3La+2Rab & -3b & 6La+4Rab \\ -3C_0'a & -6b & -6C_0'a & 6b & 6C_0'a & 3b & 3C_0'a & -3b \\ -6b & -3La+4Rab & 6b & -6La+8Rab & 3b & 6La+4Rab & -3b & 3La+2Rab \\ -3C_0'a & -3b & -6C_0'a & 3b & 6C_0'a & 6b & 3C_0'a & -6b \\ 3b & -3La+2Rab & 3b & -6La+4Rab & 6b & 6La 8Rab & -6b & 3La+4Rab \\ -6C_0'a & -3b & -3C_0'a & 3b & 3C_0'a & 6b & 6C_0'a & -6b \\ -3b & -6La+4Rab & 3b & -3La+2Rab & 6b & 3La+4Rab & -6b & 6La+8Rab \end{bmatrix}$$

$$\{\delta\}_e = [p_1, q_1, p_2, q_2, p_3, q_3, p_4, q_4]^T$$

and

$$[B]_e = \begin{bmatrix} B_{11} & 0 & B_{12} & 0 & B_{13} & 0 & B_{14} & 0 \\ 0 & 0 & 0 & 0 & 0 & 0 & 0 & 0 \\ B_{21} & 0 & B_{22} & 0 & B_{23} & 0 & B_{24} & 0 \\ 0 & 0 & 0 & 0 & 0 & 0 & 0 & 0 \\ B_{31} & 0 & B_{32} & 0 & B_{33} & 0 & B_{34} & 0 \\ 0 & 0 & 0 & 0 & 0 & 0 & 0 & 0 \\ B_{41} & 0 & B_{42} & 0 & B_{43} & 0 & B_{44} & 0 \\ 0 & 0 & 0 & 0 & 0 & 0 & 0 & 0 \end{bmatrix}$$

APPENDIX B

The method of solution for the algebraic system of equations of the obstructed tube is described here. For each of the unobstructed tube sections upstream or downstream of the stenosis the system of equations is

$$[A^*]\{\delta^*\} + [B^*]\{\delta^*\} = \{f^*\} \tag{B1}$$

The system of equations for a stenosis located at element m is

$$p^k_{2m} - p^k_{2m+2} = A\, Q^k_{2m} + B|Q^k_{2m}|Q^k_{2m} + C\,\frac{Q^k_{2m} - Q^{k-1}_{2m}}{\Delta t}\, Q^k_{2m} = Q^k_{2m+2} \tag{B2}$$

where k is the number of time increment.

The method of solution is based on the bisection method applied to (B2). The error is calculated using the following steps:

1. Guess for Q^k_{2m}.
2. Substitute Q^k_{2m} as distal boundary condition for the upstream tube section and proximal boundary condition for the downstream tube section.
3. Use the unobstructed tube method of solution to solve for p^k_{2m} and p^k_{2m+2}.
4. Calculate error given as

$$\Delta E = p^k_{2m} - p^k_{2m+2} - A\, Q^k_{2m} - B|Q^k_{2m}|Q^k_{2m} - C\,\frac{Q^k_{2m} - Q^k_{2m+2}}{\Delta t}$$

To use the bisection method, two initial flows Q_A and Q_B which yield ΔE_A and ΔE_B such that $\Delta E_A \cdot \Delta E_A < 0$ are required. To find such flows, a search routine is used. The algorithm of this search routine is

1. Let $Q_A = Q^{k-1}_{2m}$ then calculate ΔE_A

2. Let $\Delta Q = Q_{2m}^{k-1} - Q_{2m}^{k-2}$

3. Let $Q_i = Q_A \qquad i = 1$

4. Let $Q_{i+1} = Q_i + \Delta Q \qquad i = 1, 2, 3, \ldots$

5. Calculate ΔE_{i+1}

6. If $(\Delta E_{i+1})(\Delta E_A)$ $\begin{cases} <0 \text{ set } Q_B = Q_{i+1} & \text{stop bisection method} \\ >0 \text{ continue} \end{cases}$

7. If $\Delta E_A - \Delta E_{i+1}$ $\begin{cases} >0 \text{ set } i = i + 1 & \text{return to step 4} \\ <0 \text{ continue} \end{cases}$

8. Let $Q_i = Q_A$

9. Let $\Delta Q = -\Delta Q$ set $i = i + 1$ return to step 4

Once the two flows Q_A and Q_B are found, the bisection method with the following algorithm is used:

For $i = 1, 2, 3, \ldots$, repeat the steps as needed.

1. If $Q_A - Q_B$ $\begin{cases} <\varepsilon Q_A & \text{set } Q_{2m}^k = Q_A \\ >\varepsilon Q_A & \text{continue} \end{cases}$ ε is small number

2. $Q_i = \dfrac{Q_A + Q_B}{2}$

3. Calculate ΔE_i.

4. If $\Delta E_i \cdot \Delta E_A$ $\begin{cases} >0 & \text{set } Q_A = Q_i \\ <0 & \text{set } Q_B = Q_i \end{cases}$

5. $i = i + 1$ return to step 1

APPENDIX C

Figure C1. Experimental laboratory system

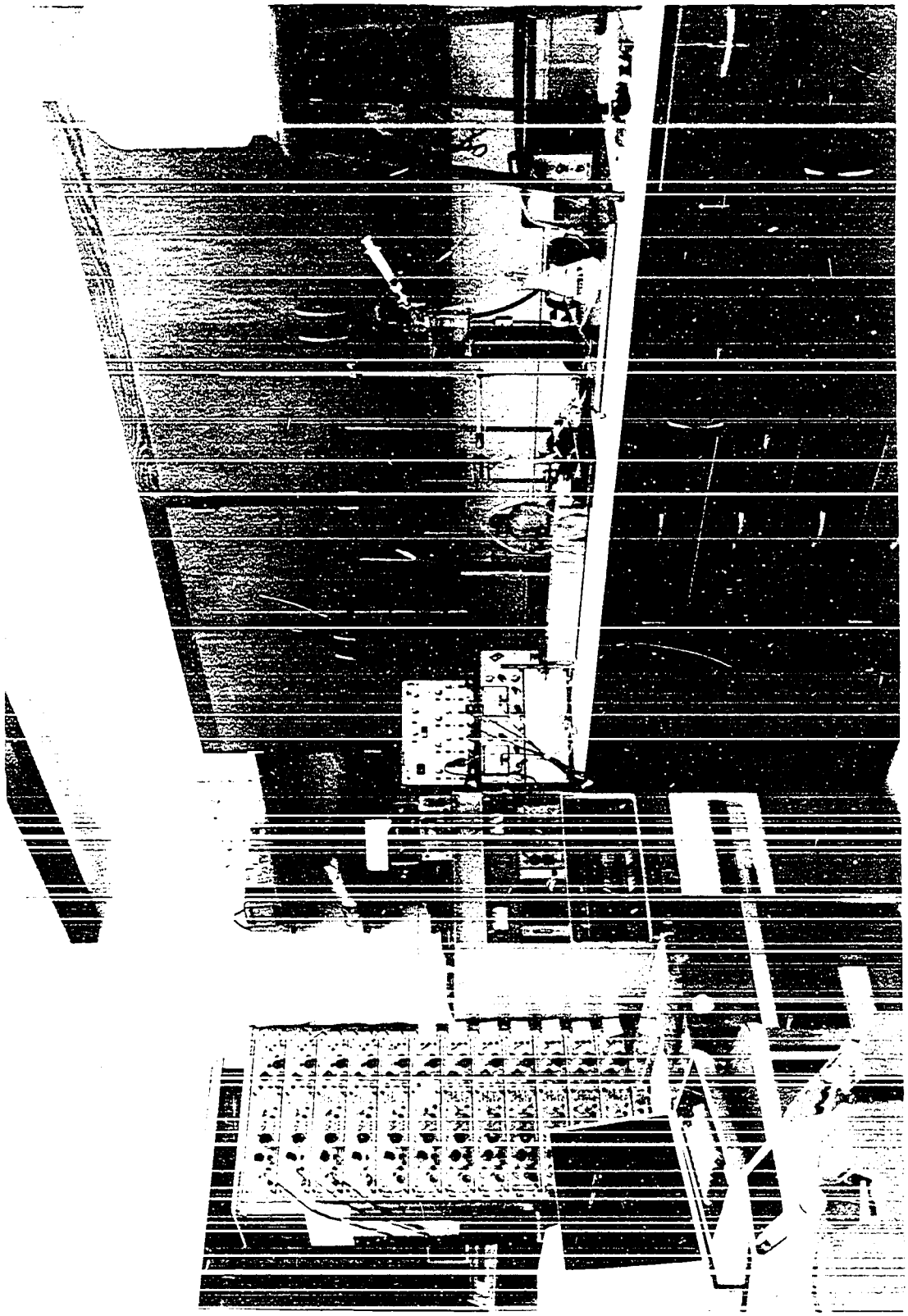

Figure C2. Latex tube test-section with strain-gage pressure transducers and electromagnetic flowmeter probes